



Article

Photocycle Dynamics of the Archaerhodopsin 3 Based Fluorescent Voltage Sensor QuasAr1

Alfons Penzkofer ^{1,*}, Arita Silapetere ² and Peter Hegemann ²

¹ Fakultät für Physik, Universität Regensburg, Universitätsstraße 31, D-93053 Regensburg, Germany

² Experimentelle Biophysik, Institut für Biologie, Humboldt Universität zu Berlin, Invalidenstraße 42, D-10115 Berlin, Germany; arita.silapetere@hu-berlin.de (A.S.); hegemann@rz.hu-berlin.de (P.H.)

* Correspondence: alfons.penzkofer@physik.uni-regensburg.de; Tel.: +49-941-943-2107

Received: 8 November 2019; Accepted: 19 December 2019; Published: 25 December 2019



Abstract: The retinal photocycle dynamics of the fluorescent voltage sensor QuasAr1 (Archaerhodopsin 3 P60S-T80S-D95H-D106H-F161V mutant from *Halorubrum sodomense*) in pH 8 Tris buffer was studied. The samples were photoexcited to the first absorption band of the protonated retinal Schiff base (PRSB) Ret₅₈₀ (absorption maximum at $\lambda_{\max} \approx 580$ nm), and the retinal Schiff base photoisomerization and protonation state changes were followed by absorption spectra recordings during light exposure and after light exposure. Ret₅₈₀ turned out to be composed of two protonated retinal Schiff base isomers, namely Ret₅₈₀_I and Ret₅₈₀_{II}. Photoexcitation of Ret₅₈₀_I resulted in barrier-involved isomerization to Ret₅₄₀ (quantum yield ≈ 0.056) and subsequent retinal proton release leading to Ret₄₁₀ deprotonated retinal Schiff base (RSB). In the dark, Ret₄₁₀ partially recovered to Ret₅₈₀_I and partially stabilized to irreversible Ret₄₀₀ due to apoprotein restructuring (Ret₄₁₀ lifetime ≈ 2 h). Photoexcitation of Ret₅₈₀_{II} resulted in barrier-involved isomerization to Ret₆₄₀ (quantum yield ≈ 0.00135) and subsequent deprotonation to Ret₃₇₀ (RSB). In the dark, Ret₃₇₀ partially recovered to Ret₅₈₀_{II} and partially stabilized to irreversible Ret₃₅₀ due to apoprotein restructuring (Ret₃₇₀ lifetime ≈ 10 h). Photocycle schemes and reaction coordinate diagrams for Ret₅₈₀_I and Ret₅₈₀_{II} were developed and photocycle parameters were determined.

Keywords: QuasAr1; Archaerhodopsin 3; genetically encoded fluorescent voltage sensor; absorption spectroscopic characterization; fluorescence studies; photocycle dynamics; photoisomerization; deprotonation; reprotonation

1. Introduction

Tracking membrane potential of cells, especially neurons, using fluorescence methods is of high interest and is an active field of research (change of membrane voltage causes change of fluorescence efficiency) [1–10]. To determine membrane voltage, a variety of voltage sensitive dyes [11–13], genetically encoded calcium indicators (GECI) [4,14,15], and genetically encoded voltage indicators (GEVI) based on voltage sensing domains (VSD, composed of four trans-membrane helices and fused fluorescent proteins) [16–20] and on microbial rhodopsins (composed of seven trans-membrane α -helices with covalently bound retinal, using the intrinsic fluorescence of retinal [9,10,21–23] or the modified fluorescence from attached fluorescent proteins [19,23,24] or dyes [12]) are in use. Often, Förster-type resonance energy transfer (FRET) is involved in dye or fluorescent protein connection to VSDs and rhodopsins [12,25].

All-optical electrophysiology in neuroscience was achieved by channelrhodopsin based optical perturbation of membrane potentials and the membrane potential readout with fluorescent voltage sensing domains [26–28].

Most microbial rhodopsin voltage indicators are based on Archaeorhodopsin 3 (Arch) from *Halorubrum sodomense* [29] and variants thereof obtained by mutations (Arch D95N [29], Arch D95N-D106E [27], Arch D95Q-D106E [30], Archer1 (=Arch D95E-T99C) [31], Archer2 (=Arch D95E-T99C-A225M) [31], QuasAr1 (=Arch P60S-T80S-D95H-D106H-F161V) [26], QuasAr2 (=QuasAr1 H95Q) [26], QuasAr3 (=QuasAr2 K171R) [28], paQuasAr3 (=QuasAr3 V59A) [28], Archon1 (=Arch T20S-G41A-V44E-P60S-T80P-D86N-D95Q-D106H-A136T-F161V-T183I-L197I-G241Q) [32], and Archon2 (=Arch T56P-P60S-T80P-D95H-T99S-T116I-F161V-T183I-L197I-A225C) [32]). The mutations improved the fluorescence intensity dependence on membrane voltage and the membrane localization [26,28,31,32].

Here, a detailed study is presented of the photocycle dynamics of QuasAr1 (“Quality superior to Arch”) in pH 8 Tris buffer to better understand the photoexcitation and relaxation dynamics affecting the behavior of the fluorescent voltage sensor.

The analysis of the photocycle dynamics revealed that Ret₅₈₀ was composed of two protonated retinal Schiff base (PRSB) isomers, named Ret_{580I} and Ret_{580II}, with different photocycle dynamics (different photoisomerization paths, isomerization yields, deprotonation rates, and protonation recoveries). Schemes of the photocycle were developed according to the experimental results. While the photoisomerization occurred on a ten picoseconds timescale, the protonated retinal Schiff base deprotonation to neutral retinal Schiff base (RSB) in the formed isomeric states occurred on a ten seconds timescale. The reprotonation to the original state was found to be slow, of the order of an hour for the reformation of Ret_{580I} and of the order of ten hours for the reformation of Ret_{580II}. The slow reformation of Ret_{580I} and Ret_{580II} was competing with thermal apoprotein restructuring leading to RSB stabilization without reprotonation. The thermal dynamics of QuasAr1 was studied in a separate paper (apparent melting temperature determination, thermal activated ground-state protonated retinal Schiff base isomerization, deprotonation, and apoprotein restructuring) [33].

2. Results

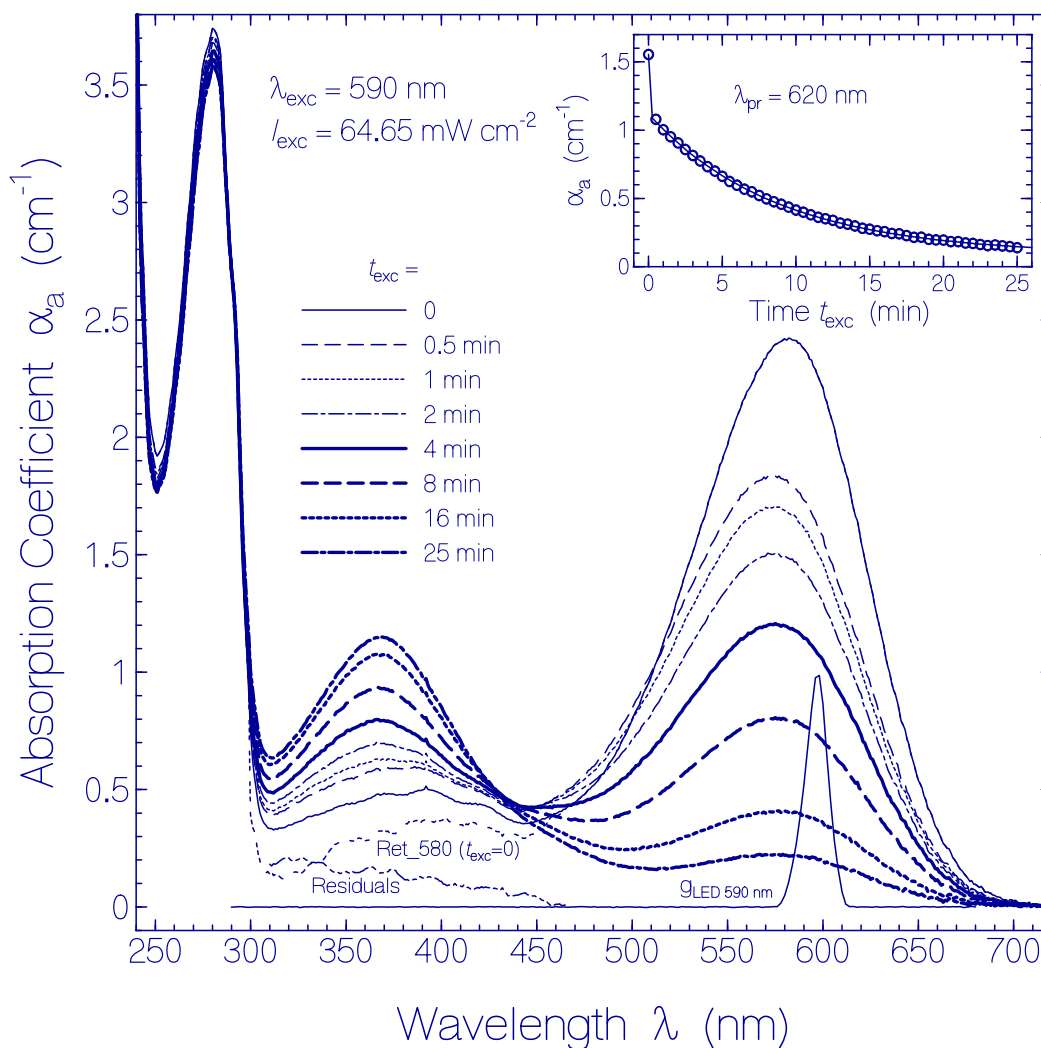
The QuasAr1 samples in pH 8 Tris buffer were photoexcited to the first absorption band (protonated retinal Schiff base Ret₅₈₀) in the green-yellow-orange spectral range, and the retinal photoisomerization and protonation state changes were followed by absorption spectra recordings during light exposure and after light exposure. The temporal absorption coefficient development at fixed wavelengths was measured with high time resolution. Additionally, excitation wavelength dependent fluorescence emission quantum distributions were measured immediately after excitation light switch-off and after sample recovery in the dark (results presented in the Supplementary Materials). Emission wavelength dependent fluorescence excitation quantum distributions were also determined after sample recovery (results are shown in the Supplementary Materials).

2.1. Absorption Spectroscopic Photocycle Studies

QuasAr1 samples were excited with light emitting diodes LED 590 nm (excitation near absorption maximum of Ret₅₈₀) and LED 530 nm (excitation near absorption maximum of protonated retinal Schiff base photoisomer Ret₅₄₀ of Ret_{580I}) as well as with a HeNe laser at 632.8 nm (excitation near absorption maximum of protonated retinal Schiff base photoisomer Ret₆₄₀ of Ret_{580II}). For the excitation with LED 590 nm, photocycle studies with three different excitation intensities were carried out to study the dependence of the photocycle dynamics on the excitation intensity. The excitations with LED 530 nm and a HeNe laser were carried out to study the influence of the excitation wavelength within the broad S₀-S₁ absorption band of the Ret₅₈₀ chromophores and of the formed photoisomer excitations on the photocycle dynamics.

The results of the photocycle studies with LED 590 nm at high excitation intensity are presented below (Figures 1–4), while the results of the photocycle studies with LED 590 nm at medium intensity (Figures S1–S3) and at low intensity (Figures S4 and S5) as well as the results of the photocycle studies with LED 530 nm (Figures S6–S9) and with the HeNe laser (Figures S10–S13) are presented in the Supplementary Materials.

In Figure 1a, the development of absorption coefficient spectra of QuasAr1 in pH 8 buffer during light exposure with LED 590 nm ($\lambda_{\text{exc}} = 590 \text{ nm}$) of input intensity $I_{\text{exc}} = 64.65 \text{ mW cm}^{-2}$ is displayed. The spectral light distribution $g_{\text{LED 590 nm}}(\lambda)$ of the LED 590 nm is included in the figure. The absorption coefficient curves belong to the exposure times listed in the legend. With increasing exposure time, the curves show the decrease of the absorption band around 580 nm and the dominant buildup of an absorption band around 370 nm. The triple-dotted curve belonging to $t_{\text{exc}} = 0$ (named Ret_580 ($t_{\text{exc}} = 0$)) shows the initial absorption coefficient spectrum of QuasAr1 deprived from retinal isomer contributions other than Ret_580 (dashed triple dotted curve named Residuals). The curves Ret_580 ($t_{\text{exc}} = 0$) and Residuals were determined in [33]. The inset in Figure 1a shows the temporal development of the absorption coefficient $\alpha_a(t_{\text{exc}})$ at the probe wavelength $\lambda_{\text{pr}} = 620 \text{ nm}$ (long-wavelength absorption region of Ret_580_I component) followed by a slow absorption decrease (photoconversion of Ret_580_{II} component).



(a)

Figure 1. Cont.

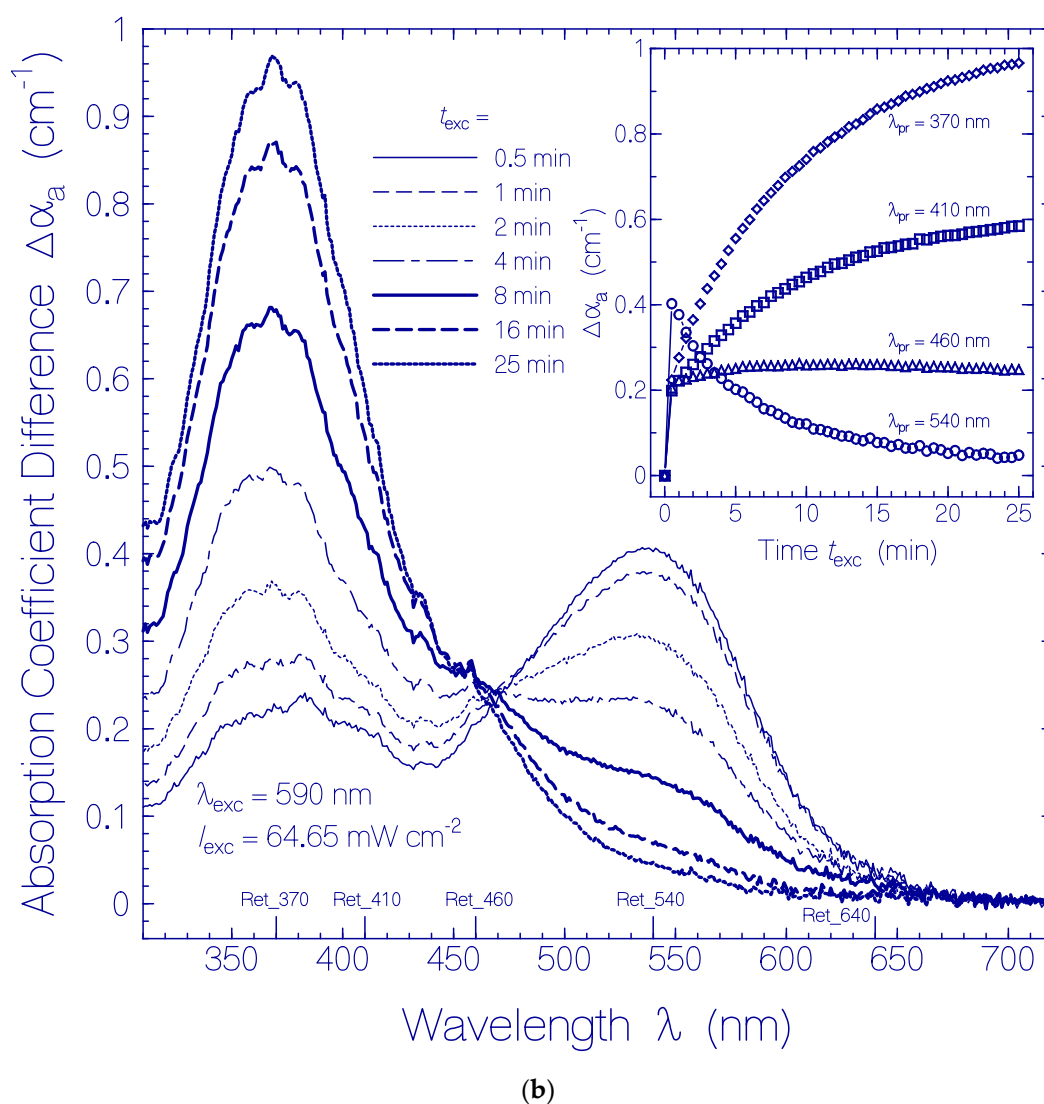


Figure 1. (a) Development of absorption coefficient spectra of a QuasAr1 sample in pH 8 Tris buffer during light exposure with LED 590 nm with input excitation intensity of $I_{\text{exc}} = 64.65 \text{ mW cm}^{-2}$. The durations of light exposure are listed in the figure. The triple dotted curve named Ret_580 ($t_{\text{exc}} = 0$) in the wavelength range $>310 \text{ nm}$ shows the absorption coefficient contribution of Ret_580 to QuasAr1 before light exposure (taken from Figure 1 in [33]). The dashed triple-dotted curve named Residuals shows the absorption coefficient contribution of residual retinal isomers in QuasAr1 other than Ret_580 (taken from Figure 1 in [33]). The curve $g_{\text{LED } 590 \text{ nm}}(\lambda) = S_{\text{LED } 590 \text{ nm}}(\lambda)/S_{\text{LED } 590 \text{ nm}}(\lambda_{\text{max}})$ shows the spectral distribution of the excitation light source LED 590 nm. The inset shows the temporal dependence of α_a (620 nm) versus exposure time t_{exc} . The data points are fitted by $\alpha_a(t_{\text{exc}}) = \alpha_a(0) - \Delta\alpha_I[1 - \exp(-t_{\text{exc}}/\tau_{\text{sat},I})] - \Delta\alpha_{II}[1 - \exp(-t_{\text{exc}}/\tau_{\text{sat},II})]$ with $\alpha_a(0) = 1.554 \text{ cm}^{-1}$, $\Delta\alpha_I = 0.436 \text{ cm}^{-1}$, $\tau_{\text{sat},I} = 0.015 \text{ min}$, $\Delta\alpha_{II} = 1.03 \text{ cm}^{-1}$, and $\tau_{\text{sat},II} = 8.65 \text{ min}$. (b) Absorption coefficient spectra of formed species of QuasAr1 in pH 8 Tris buffer due to light exposure with LED 590 nm of input intensity $I_{\text{exc}} = 64.65 \text{ mW cm}^{-2}$. The absorption contributions of Ret_580, $\alpha_{\text{aRet}_580}(\lambda, t_{\text{exc}})$, and of the initial residuals, $\alpha_{\text{a,Residuals}}(\lambda, 0)$, from (a) are subtracted, i.e., $\Delta\alpha_a(\lambda, t_{\text{exc}}) = \alpha_a(\lambda, t_{\text{exc}}) - \alpha_{\text{aRet}_580}(\lambda, t_{\text{exc}}) - \alpha_{\text{a,Residuals}}(\lambda, t_{\text{exc}} = 0)$. The approximate peak wavelength positions of the retinal isomers Ret_640, Ret_540, Ret_460, Ret_410, and Ret_370 are indicated at the bottom. The inset shows the temporal development of $\Delta\alpha_a$ at $\lambda_{\text{pr}} = 540 \text{ nm}$, 460 nm, 410 nm, and 370 nm versus exposure time t_{exc} .

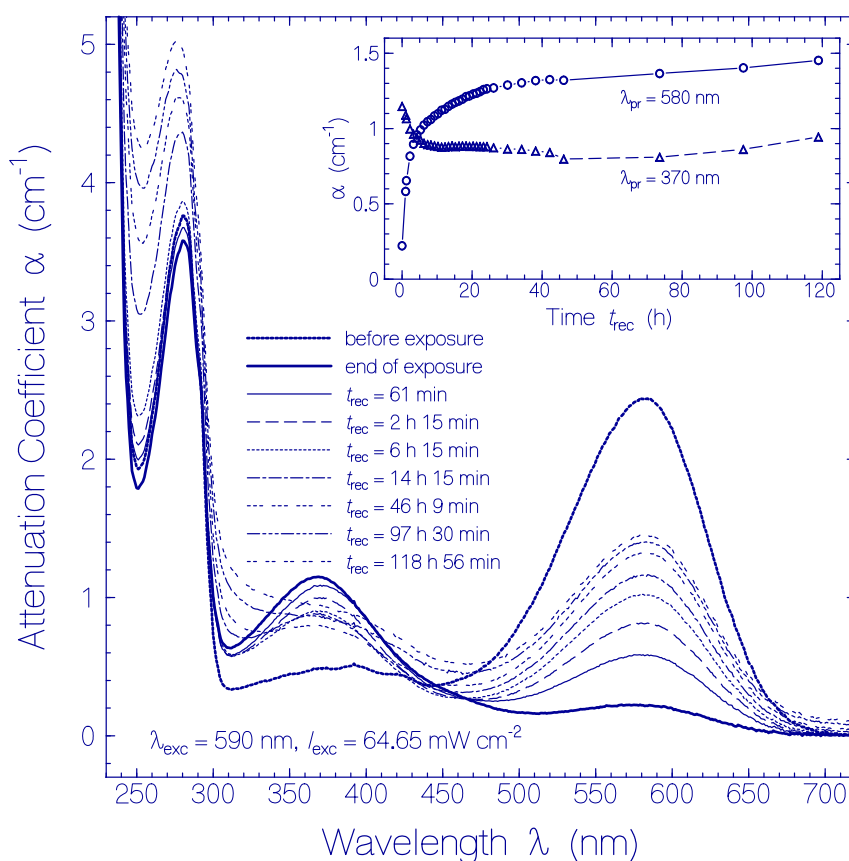


Figure 2. Attenuation coefficient spectra recovery of QuasAr1 in pH 8 Tris buffer after light exposure with LED 590 nm (input excitation intensity $I_{\text{exc}} = 64.65 \text{ mW cm}^{-2}$) for an exposure time of $t_{\text{exc}} = 25 \text{ min}$ (see Figure 1a). The durations of recovery t_{rec} are listed in the Figure. The attenuation coefficient spectra before exposure ($t_{\text{exc}} = 0$) and at end of exposure ($t_{\text{exc}} = 25 \text{ min}$) are included. The inset shows the attenuation coefficient recovery $\alpha(t_{\text{rec}})$ at $\lambda_{\text{pr}} = 580 \text{ nm}$ and 370 nm .

More detailed information on the photoinduced retinal isomerization and deprotonation dynamics of Ret_580 during light exposure was obtained by subtracting the remaining Ret_580 absorption coefficient contributions $\alpha_{a,\text{Ret}_580}(\lambda, t_{\text{exc}})$ at time t_{exc} and the initial residual retinal isomers contributions Residuals from the developing absorption coefficient spectra of Figure 1a. The remaining Ret_580 absorption coefficient contributions are approximately determined by $\alpha_{a,\text{Ret}_580}(\lambda, t_{\text{exc}}) \approx \alpha_{a,\text{Ret}_580}(\lambda, t_{\text{exc}} = 0) \times \alpha_a(\lambda = 620 \text{ nm}, t_{\text{exc}}) / \alpha_a(\lambda = 620 \text{ nm}, t_{\text{exc}} = 0)$ (the spectral shape of $\alpha_{a,\text{Ret}_580}$ is assumed to do not change with exposure time, the magnitude of $\alpha_{a,\text{Ret}_580}(\lambda = 620 \text{ nm}, t_{\text{exc}})$ is nearly given by the magnitude of $\alpha_a(\lambda = 620 \text{ nm}, t_{\text{exc}})$ of QuasAr1 since at $\lambda = 620 \text{ nm}$ absorption contributions from formed species are thought to be small). The resulting curves $\Delta\alpha_a(\lambda, t_{\text{exc}}) = \alpha_a(\lambda, t_{\text{exc}}) - \alpha_{a,\text{Ret}_580}(\lambda, t_{\text{exc}}) - \alpha_{a,\text{Residuals}}(\lambda, t_{\text{exc}} = 0)$, which are displayed in the main part of Figure 1b, show the absorption coefficient spectra development of formed species of QuasAr1 due to the light exposure. New absorption bands are seen around $\lambda \approx 540 \text{ nm}$ (PRSB Ret_540), $\approx 460 \text{ nm}$ (PRSB Ret_460), $\approx 410 \text{ nm}$ (RSB Ret_410), and $\approx 370 \text{ nm}$ (RSB Ret_370). There is an indication of a new absorption band around 640 nm (PRSB Ret_640). The absorption band of Ret_540 extends out beyond $\lambda_{\text{exc}} = 590 \text{ nm}$. The temporal developments of $\Delta\alpha_a$ at the probe wavelengths $\lambda_{\text{pr}} = 540 \text{ nm}$, 460 nm , 410 nm , and 370 nm are depicted in the inset of Figure 1b. The absorption band of Ret_540 decreased with continued light exposure. It is thought that Ret_540 is formed by photoisomerization of PRSB Ret_580_I (likely 13-*cis* isomer in specific apoprotein conformation Apoprotein_I) to PRSB Ret_540 (likely all-*trans* isomer in apoprotein conformation Apoprotein_I). The decrease of Ret_540 for $t_{\text{exc}} > 30 \text{ s}$ is thought to be determined dominantly by deprotonation of Ret_540 to Ret_410. The absorption bands

of Ret_460, Ret_410, and Ret_370 are overlapping. Ret_370 was built up during the whole time of light exposure. It is thought that Ret_580_{II} (likely all-*trans* isomer in specific apoprotein conformation Apoprotein_{II}) is converted to Ret_370 (likely formed by photoisomerization of all-*trans* retinal isomer to a *cis* isomer Ret_640 in specific apoprotein conformation Apoprotein_{II} and subsequent deprotonation, for details see discussion below). At $\lambda_{pr} = 460$ nm the absorption changes are dominated by the short-wavelength tail of Ret_540 and the long-wavelength tails of Ret_410 and Ret_370. The build-up of Ret_460 population is small and only indicated by a small absorption structure change around 460 nm.

The attenuation coefficient spectra development of the QuasAr1 sample used in Figure 1a after excitation light switch-off over a recovery time range of nearly five days (sample in the dark at room temperature) is displayed in Figure 2. The inset in Figure 2 shows the temporal attenuation coefficient development at $\lambda_{pr} = 580$ nm and 370 nm.

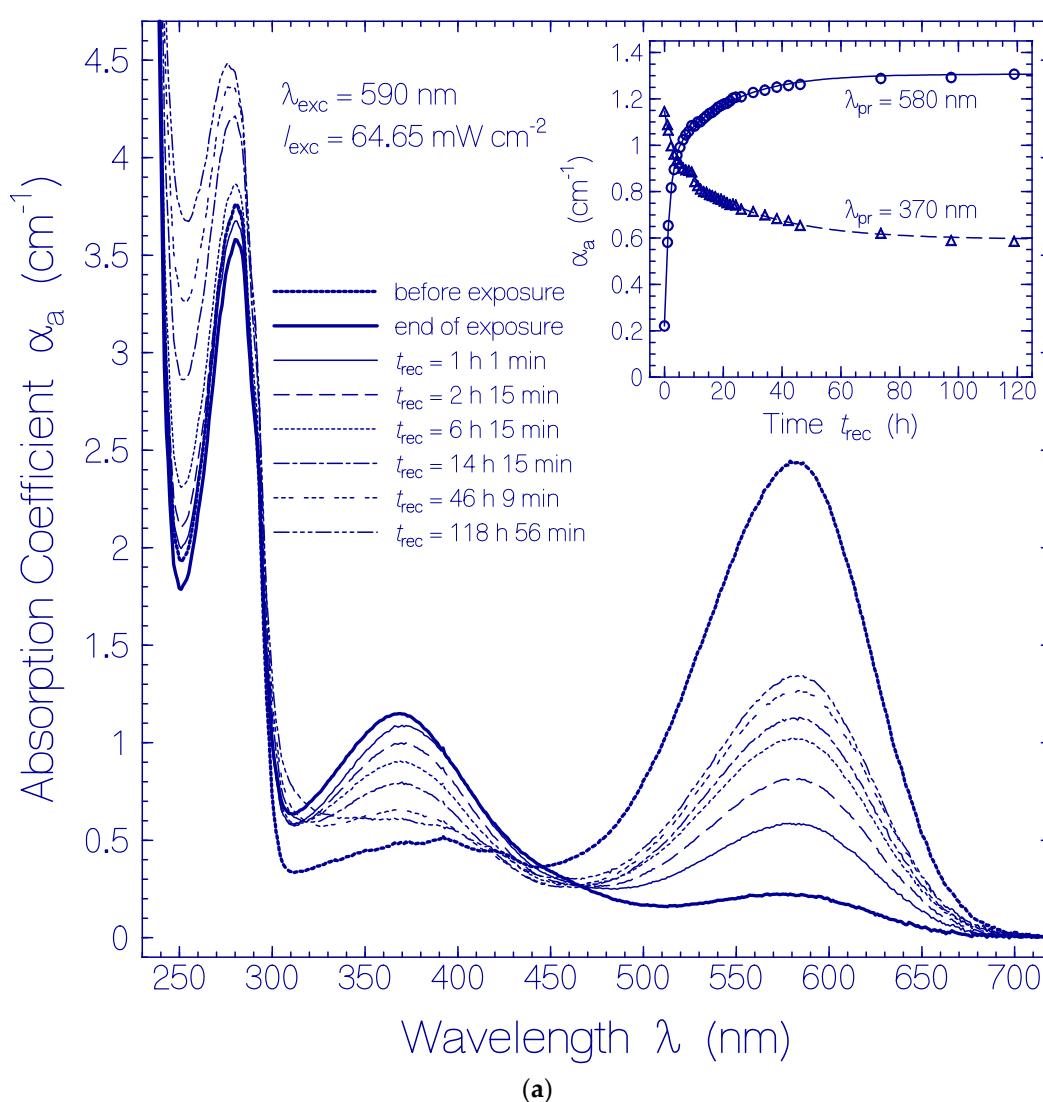


Figure 3. Cont.

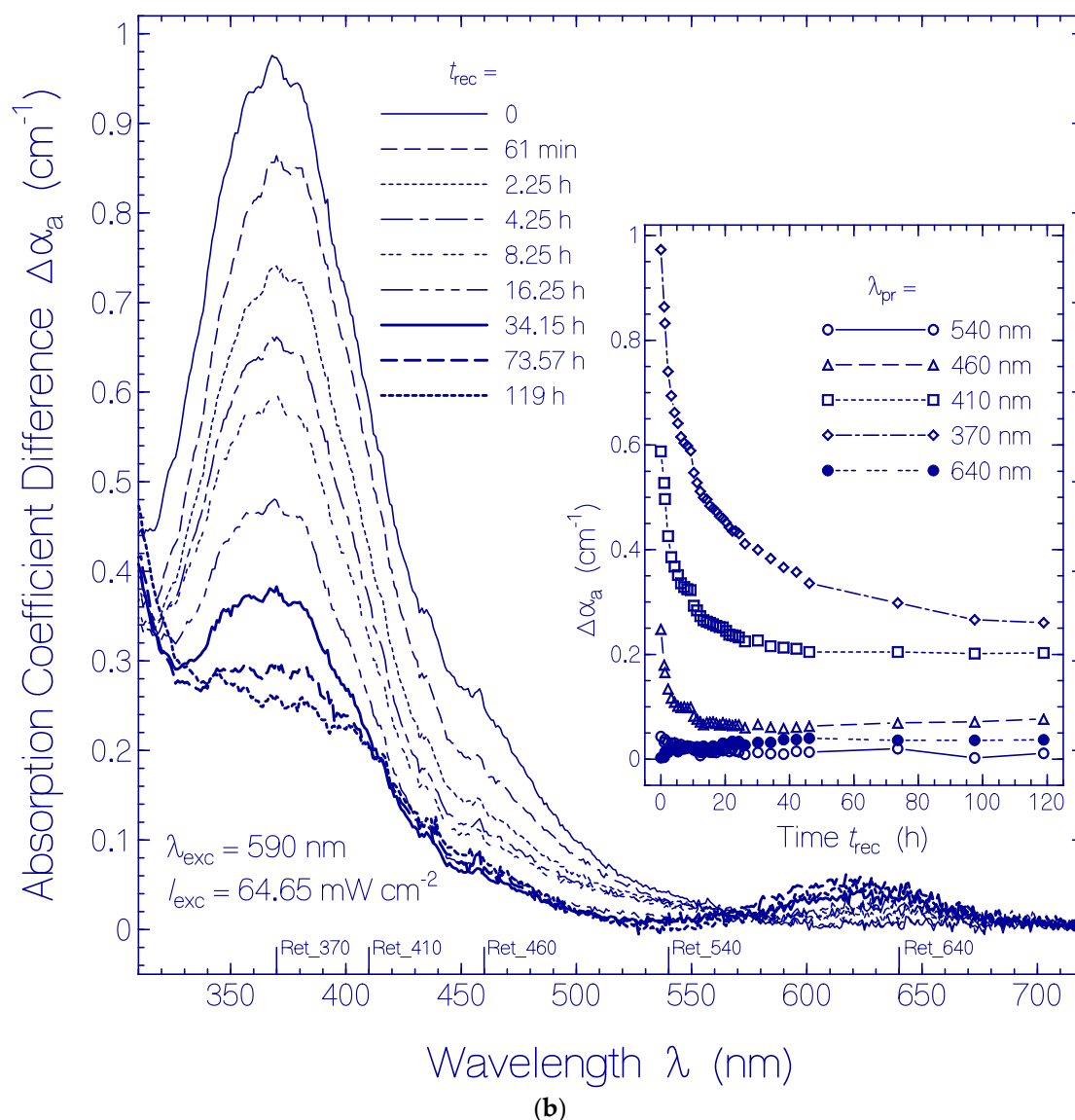


Figure 3. (a) Absorption coefficient spectra recovery of QuasAr1 in pH 8 Tris buffer after light exposure with LED 590 nm (input excitation intensity $I_{exc} = 64.65$ mW cm⁻²) for an exposure time of $t_{exc} = 25$ min (see Figure 1a). Immediately after the end of exposure, fluorescence emission spectra were measured. The durations of recovery t_{rec} are listed in the figure. The absorption coefficient spectra before exposure ($t_{exc} = 0$) and at the end of exposure ($t_{exc} = 25$ min) are included. The inset shows the absorption coefficient recoveries $\alpha_a(t_{rec})$ at $\lambda_{pr} = 580$ nm and 370 nm. The data points are fitted by $\alpha_a(t_{rec}) = \alpha_a(0) + \Delta\alpha_I[1 - \exp(-t_{rec}/\tau_{rec,I})] + \Delta\alpha_{II}[1 - \exp(-t_{rec}/\tau_{rec,II})]$ with $\alpha_a(0, 580$ nm) = 0.22 cm⁻¹, $\Delta\alpha_I(580$ nm) = 0.71 cm⁻¹, $\tau_{rec,I}(580$ nm) = 1.52 h, $\Delta\alpha_{II}(580$ nm) = 0.376 cm⁻¹, $\tau_{rec,II}(580$ nm) = 19.26 h, $\alpha_a(0, 370$ nm) = 1.15 cm⁻¹, $\Delta\alpha_I(370$ nm) = -0.195 cm⁻¹, $\tau_{rec,I}(370$ nm) = 2.96 h, $\Delta\alpha_{II}(370$ nm) = -0.358 cm⁻¹, and $\tau_{rec,II}(370$ nm) = 26.7 h. (b) Absorption coefficient difference spectra development $\Delta\alpha_a(\lambda, t_{rec}) = \alpha_a(\lambda, t_{rec}) - \alpha_{a,Ret_{580}}(\lambda, t_{rec}) - \alpha_{a,Residuals}(\lambda, t_{exc} = 0)$ of QuasAr1 in pH 8 Tris buffer after light exposure with LED 590 nm of input intensity $I_{exc} = 64.65$ mW cm⁻² for 25 min. The inset shows the temporal development of $\Delta\alpha_a$ at $\lambda_{pr} = 640$ nm, 540 nm, 460 nm, 410 nm, and 370 nm versus recovery time t_{rec} .

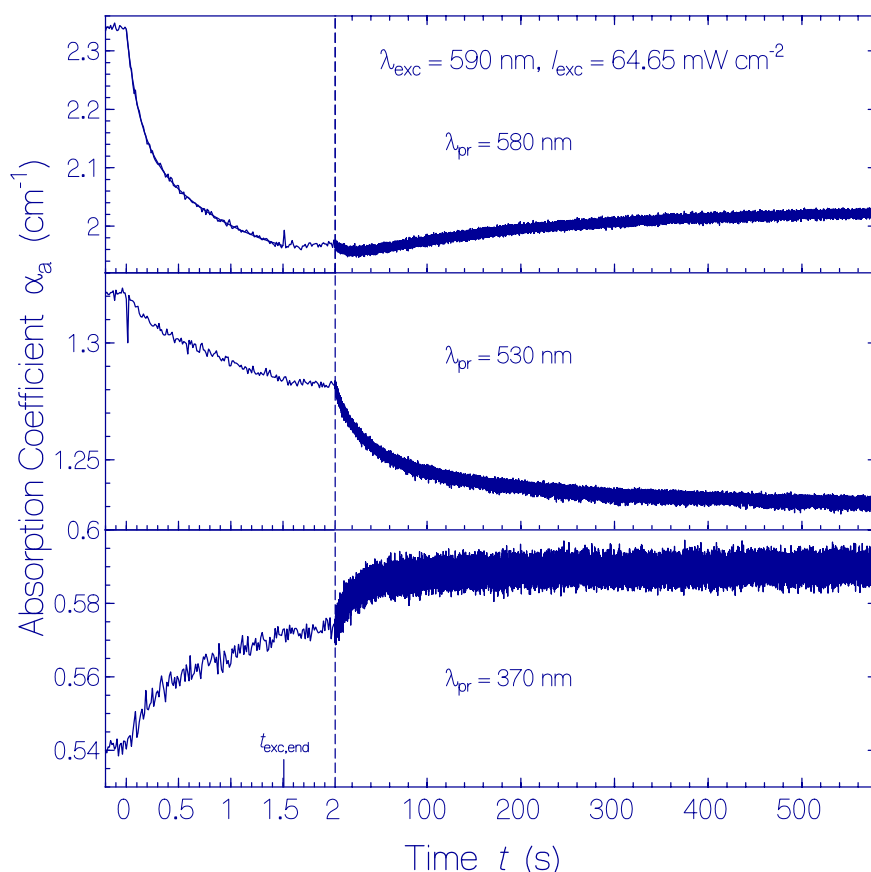


Figure 4. Temporal absorption coefficient development of QuasAr1 in pH 8 Tris buffer at the probe wavelengths $\lambda_{pr} = 580$ nm (top part, peak absorption of Ret_580), 530 nm (middle part, near peak absorption of Ret_540), and 370 nm (bottom part, peak absorption of Ret_370) before, during, and after photoexcitation with LED 590 nm of excitation intensity $I_{exc} = 64.65 \text{ mW cm}^{-2}$ for a duration of $t_{exc} = 1.5$ s. The same sample was used. Immediately after measurement at $\lambda_{pr} = 580$ nm, the measurement was continued at $\lambda_{pr} = 530$ nm, and then, at $\lambda_{pr} = 370$ nm. In the top left subfigure, the data points during light exposure are fitted by $\alpha_a(t_{exc}) = \alpha_a(0) - \Delta\alpha_{a,I}[1 - \exp(-t_{exc}/\tau_I)] - \Delta\alpha_{a,II}[1 - \exp(-t_{rec}/\tau_{II})]$ with $\alpha_a(0) = 2.34 \text{ cm}^{-1}$, $\Delta\alpha_{a,I} = 0.172 \text{ cm}^{-1}$, $\tau_I = 116 \text{ ms}$, $\Delta\alpha_{a,II} = 0.245 \text{ cm}^{-1}$, and $\tau_{II} = 907 \text{ ms}$. A fit of the right part of the middle subfigure with $\alpha_a(t > t_{exc,end}) = \alpha_a(t_{exc,end}) - \Delta\alpha_a[1 - \exp(-(t - t_{exc,end})/\tau_{rel,Ret_540})]$ gives $\alpha_a(t_{exc,end}) = 1.284 \text{ cm}^{-1}$, $\Delta\alpha_a = 0.0425 \text{ cm}^{-1}$, and $\tau_{rel,Ret_540} = 37 \text{ s}$. A fit of the right part of the bottom subfigure with $\alpha_a(t > t_{exc,end}) = \alpha_a(t_{exc,end}) + \Delta\alpha_a[1 - \exp(-(t - t_{exc,end})/\tau_{rel,Ret_640})]$ gives $\alpha_a(t_{exc,end}) = 0.571 \text{ cm}^{-1}$, $\Delta\alpha_a = 0.017 \text{ cm}^{-1}$, and $\tau_{rel,Ret_640} = 19.3 \text{ s}$.

The corresponding absorption coefficient spectra development (scattering contributions approximately subtracted) is shown in Figure 3a. The absorption band centered at 580 nm (Ret_580) recovered partly, and the formed absorption band around 370 nm (Ret_370 including Ret_410) disappeared partly. The absorption band around 280 nm (dominant tryptophan absorption) increased steadily due to thermal apoprotein restructuring [33]. The inset in Figure 3a shows the partial absorption coefficient recovery at $\lambda_{pr} = 580$ nm where the absorption is determined by Ret_580, and the partial absorption coefficient decrease at $\lambda_{pr} = 370$ nm due to reprotonation of Ret_370 to Ret_580. The only partial reconversion of Ret_370 to Ret_580 is due to a changeover from the reversible photocycle dynamics to the thermal irreversible deprotonation of Ret_580 and the Ret_370 ground-state potential energy lowering below the ground-state energy level of Ret_580 (changeover from Ret_370 to Ret_350, see discussion below) caused by the dynamic thermal apoprotein restructuring [33] during the slow recovery time of the photocycle process.

In order to see details in the absorption coefficient spectra development after excitation light switch-off in Figure 3a, the absorption coefficient spectra development $\Delta\alpha_a(\lambda, t_{rec}) = \alpha_a(\lambda, t_{rec}) - \alpha_{a,Ret_580}(\lambda, t_{rec}) - \alpha_{a,Residuals}(\lambda, t_{exc} = 0)$ is displayed in Figure 3b (Ret_580 contribution and initial residual retinal contributions are subtracted from Figure 3a). The inset of Figure 3b shows the temporal development of $\Delta\alpha_a(t_{rec})$ at the probe wavelengths $\lambda_{pr} = 540$ nm, 460 nm, 410 nm, 370 nm, and 640 nm. The absorption of Ret_370, Ret_410, and Ret_460 decreased within the first 20 h of light switch-off and then leveled off. $\Delta\alpha_a(640 \text{ nm}, t_{rec})$ indicates the formation of Ret_640 by thermal activation of isomerization of Ret_580_{II} [33].

The temporal absorption coefficient developments with a time resolution of $\delta t_{res} = 12.5$ ms at $\lambda_{pr} = 580$ nm, 530 nm, and 370 nm are displayed in Figure 4 for a QuasAr1 sample in pH 8 Tris buffer. A fresh thawed sample was used. In the first run, the probe wavelength was set to $\lambda_{pr} = 580$ nm, the exposure time was $t_{exc} = 1.5$ s, and the time of recovery in the dark was set to 10 min. Then, it was followed immediately by the second run with the same exposure/dark parameters at $\lambda_{pr} = 530$ nm. Next, it was followed immediately by the third run with the same exposure/dark parameters at $\lambda_{pr} = 370$ nm.

The top part of Figure 4 shows the absorption development at $\lambda_{pr} = 580$ nm during and after light exposure. During light exposure, the absorption decreased dominantly by photoisomerization of Ret_580_I to Ret_540. After excitation light switch-off, initially a minute absorption decrease is observed likely due to the conversion of Ret_540 to Ret_410 (absorption band of Ret_540 extends out to 580 nm). The following slight absorption increase is thought to be due to partial reprotonation of Ret_410 to Ret_580_I (see discussion below).

The middle part of Figure 4 shows the absorption development at $\lambda_{pr} = 530$ nm in a second exposure of the sample. The absorption decrease during light exposure is due to the absorption decrease of the broad absorption band of Ret_580 which dominates the absorption at 530 nm. The weaker absorption decrease, as compared with $\lambda_{pr} = 580$ nm, is due to the formation of the absorption band of Ret_540 during light exposure. After light switch-off, the absorption at 530 nm decreased because of deprotonation of Ret_540 to Ret_410 (time constant $\tau_{rel,Ret_540} \approx 37$ s, see discussion below). The spike at the position of light switch-on is thought to be an artifact caused by a photoinduced transient thermal grating [34,35] (the same effect was observed by replacing the QuasAr1 sample with a sample of rhodamine 6G in methanol).

The bottom part of Figure 4 shows the absorption development at $\lambda_{pr} = 370$ nm in a third exposure of the sample. After excitation light switch-on, the increase of absorption is slightly time delayed (≈ 0.1 s). After excitation light switch-off ($t_{exc,end} = 1.5$ s), the absorption continues to increase within the first 40 s, and then, levels off (time constant $\tau_{rel,Ret_640} \approx 17$ s). The absorption dynamics is thought to be dominated by the conversion of Ret_640 to Ret_370 by proton release (see discussion below).

2.2. Quantum Yield of Photoconversion

The quantum yield of photoconversion ϕ_{con} of Ret_580 to other retinal isomers during light exposure is given [36] by the ratio of the number density ΔN_{con} of converted Ret_580 molecules to the number density $\Delta n_{ph,abs}$ of absorbed photons by Ret_580, i.e.,

$$\phi_{con} = \frac{\Delta N_{con}}{\Delta n_{ph,abs}} \quad (1)$$

The number density ΔN_{con} is determined by

$$\Delta N_{con} = N_0 \frac{\Delta\alpha_a(\lambda_{pr})}{\alpha_{a,0}(\lambda_{pr})} \quad (2)$$

where N_0 is the initial number density of Ret_580, $\alpha_{a,0}(\lambda_{pr})$ is the initial absorption coefficient of Ret_580 at the probe wavelength λ_{pr} , and $\Delta\alpha_a(\lambda_{pr})$ is the absorption coefficient change of Ret_580 at λ_{pr} (λ_{pr} is selected at a wavelength region where practically only Ret_580 is absorbing).

The initial number density N_0 of Ret_580 is given by

$$N_0 = \frac{\alpha_{a,0}(\lambda_{pr})}{\sigma_a(\lambda_{pr})} \quad (3)$$

where $\sigma_a(\lambda_{pr})$ is the absorption cross-section of Ret_580 at λ_{pr} . It is presented in Figure S2 of the Supplementary Materials to [33].

The number density $\Delta n_{ph,abs}$ of absorbed photons by Ret_580 is determined by the excitation light intensity I_{exc} at the excitation wavelength λ_{exc} , the time interval of light exposure δt_{exc} and the absorption coefficient $\alpha_a(\lambda_{exc})$ of Ret_580. It is given by

$$\Delta n_{ph,abs} = \frac{I_{exc}\delta t_{exc}}{h\nu_{exc}} \alpha_a(\lambda_{exc}) \quad (4)$$

where $h\nu_{exc}$ is the photon excitation energy ($\nu_{exc} = c_0/\lambda_{exc}$ is the photon frequency, c_0 is the speed of light in vacuum, and h is the Planck constant).

The determined approximate quantum yields of photoconversion of Ret_580 versus exposure time are displayed in Figure 5. The $\phi_{con}(t_{exc})$ curves give only approximate values of $\phi_{con,Ret_580}(t_{exc})$ since $\alpha_a(\lambda_{pr},t_{exc})$ used in the calculations is only approximately equal to $\alpha_{a,Ret_580}(\lambda_{pr},t_{exc})$, and the used $\alpha_a(\lambda_{exc},t_{exc})$ is only approximately equal to $\alpha_{a,Ret_580}(\lambda_{exc},t_{exc})$. In the main subfigures, $\lambda_{pr} = 620$ nm was used where $\alpha_a(\lambda_{pr},t_{exc})$ is nearly equal to $\alpha_{a,Ret_580}(\lambda_{pr},t_{exc})$ during the whole exposure time. In the insets of the subfigures, $\lambda_{pr} = 580$ nm was used. There, $\alpha_a(t_{exc})$ was measured with high time resolution and for the short exposure times $\alpha_a(\lambda_{pr},t_{exc})$ remained nearly equal to $\alpha_{a,Ret_580}(\lambda_{pr},t_{exc})$. The absorption coefficient data in the insets of Figure 1a ($\lambda_{exc} = 590$ nm, $I_{exc} = 64.65$ mW cm⁻², and $\lambda_{pr} = 620$ nm), Figure S1a ($\lambda_{exc} = 590$ nm, $I_{exc} = 14.07$ mW cm⁻², and $\lambda_{pr} = 620$ nm), Figure S4a ($\lambda_{exc} = 590$ nm, $I_{exc} = 1.12$ mW cm⁻², and $\lambda_{pr} = 620$ nm), Figure S6a ($\lambda_{exc} = 530$ nm, $I_{exc} = 114.2$ mW cm⁻², and $\lambda_{pr} = 620$ nm), and Figure S10a ($\lambda_{exc} = 632.8$ nm, $I_{exc} = 15.56$ mW cm⁻², and $\lambda_{pr} = 620$ nm) were employed for the main subfigures. The absorption coefficient curves in the top left parts of Figure 4 ($\lambda_{exc} = 590$ nm, $I_{exc} = 64.65$ mW cm⁻², and $\lambda_{pr} = 580$ nm), Figure S9 ($\lambda_{exc} = 530$ nm, $I_{exc} = 114.2$ mW cm⁻², and $\lambda_{pr} = 580$ nm), and Figure S13 ($\lambda_{exc} = 632.8$ nm, $I_{exc} = 15.65$ mW cm⁻², and $\lambda_{pr} = 580$ nm) were employed for the insets in the subfigures.

All $\phi_{con}(t_{exc})$ curves in Figure 5 show an initially fast decrease and a changeover to a near exposure time independent but excitation light intensity dependent low value. As was shown in [33] and is discussed below, Ret_580 consists of two protonated retinal Schiff base isomers Ret_580_I (fraction $\kappa_{Ret_580I} \approx 0.41$ [33]) and Ret_580_{II} (fraction $\kappa_{Ret_580II} \approx 0.59$ [33]) with different ground-state isomerization dynamics [33] and photoisomerization dynamics. The initially large quantum yield of photoconversion is due to the photoisomerization of Ret_580_I to Ret_540 and subsequent deprotonation of Ret_540 to Ret_410. The low quantum yield of photoconversion after conversion of Ret_580_I is due to the low-efficient photoisomerization of Ret_580_{II} to Ret_640 and subsequent deprotonation to Ret_370. The excitation intensity dependent lowering of $\phi_{con}(t_{exc})$ for $t_{exc} > 0$ is due to the generation of the photoisomers Ret_540 and Ret_640 and their subsequent back photoisomerization of Ret_540 to Ret_580_I and Ret_640 to Ret_580_{II} (see discussion below).

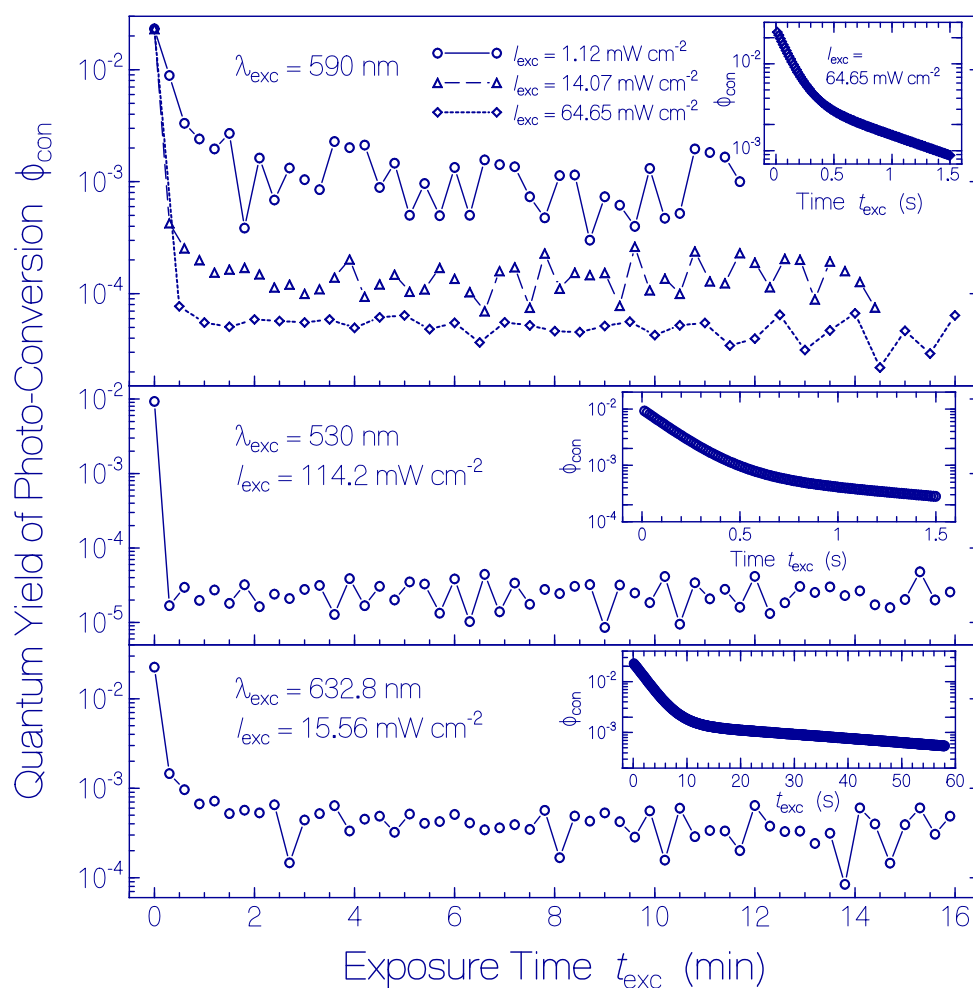


Figure 5. Quantum yield of photoconversion ϕ_{con} of Ret_580 of QuasAr1 in pH 8 Tris buffer to other retinal isomers during light exposure. (**Top part**) Photoexcitation with LED 590 nm using listed input light intensities (values derived from Figure 1a, Figures S1a and S4a). (**Middle part**) Photoexcitation with LED 530 nm using excitation intensity of $I_{exc} = 114.2 \text{ mW cm}^{-2}$ (values derived from Figure S6a). (**Bottom part**) Photoexcitation with He-Ne laser using $I_{exc} = 15.56 \text{ mW cm}^{-2}$ (values derived from Figure S10a). The curves in the insets are derived from the high time resolution absorption measurements (top part of Figure 4 for $\lambda_{exc} = 590 \text{ nm}$, top part of Figure S9 for $\lambda_{exc} = 530 \text{ nm}$, and top part of Figure S13 for $\lambda_{exc} = 632.8 \text{ nm}$).

In the top part of Figure 5, the photoconversion of Ret_580 at $\lambda_{exc} = 590 \text{ nm}$ is displayed for three different excitation intensities. The initial quantum yield of photoconversion (for $t_{exc} \rightarrow 0$) is excitation intensity independent. It is $\phi_{con}(t_{exc} = 0) = \phi_{con,Ret_{580I}}(t_{exc} = 0)\kappa_{Ret_{580I}} + \phi_{con,Ret_{580II}}(t_{exc} = 0)\kappa_{Ret_{580II}} \approx \phi_{con,Ret_{580I}}(t_{exc})\kappa_{Ret_{580I}} \approx 0.023$ giving $\phi_{con,Ret_{580I}}(t_{exc} = 0) \approx 0.056$. After complete photoconversion of Ret_580I ($t_{exc} > 1 \text{ min}$), the quantum yield of photoconversion is $\phi_{con}(t_{exc} > 1 \text{ min}, I_{exc}) \approx \phi_{con,Ret_{580II}}(I_{exc})$ which depends on the photoexcitation intensity. We find $\phi_{con,Ret_{580II}}(I_{exc} = 1.12 \text{ mW cm}^{-2}) = (1.19 \pm 0.11) \times 10^{-3}$, $\phi_{con,Ret_{580II}}(I_{exc} = 14.07 \text{ mW cm}^{-2}) = (1.38 \pm 0.084) \times 10^{-4}$, and $\phi_{con,Ret_{580II}}(I_{exc} = 64.65 \text{ mW cm}^{-2}) = (4.53 \pm 0.31) \times 10^{-5}$. This behavior is thought to be due to the low initial quantum yield of photoconversion $\phi_{con,Ret_{580II}}(t_{exc} \rightarrow 0, I_{exc} \rightarrow 0)$ and the excitation intensity dependent back photoisomerization of Ret_640 to Ret_580II (see discussion below).

In the middle part of Figure 5, the approximate photoconversion of Ret_580 is displayed for $\lambda_{exc} = 530 \text{ nm}$ and $I_{exc} = 114.2 \text{ mW cm}^{-2}$. The initial quantum yield of photoconversion is $\phi_{con}(t_{exc} = 0) \approx \phi_{con,Ret_{580I}}(t_{exc} = 0)\kappa_{Ret_{580I}} \approx 0.0093$ giving $\phi_{con,Ret_{580I}}(t_{exc}) \approx 0.023$. For $\lambda_{exc} = 530 \text{ nm}$ the photoconversion of Ret_580I is lower than that for $\lambda_{exc} = 590 \text{ nm}$ indicating some excitation

wavelength influence on the photoisomerization efficiency. After complete photoconversion of Ret_580_I ($t_{exc} > 0.5$ min) the quantum yield of photoconversion is $\phi_{con}(t_{exc} > 0.5 \text{ min}, I_{exc} = 114.2 \text{ mW cm}^{-2}) \approx \phi_{con,Ret_580_{II}}(I_{exc} = 114.2 \text{ mW cm}^{-2}) = (2.43 \pm 0.143) \times 10^{-5}$, due to the excitation intensity dependent back photoisomerization of Ret_640 to Ret_580_{II} (see discussion below).

In the bottom part of Figure 5, the photoconversion of Ret_580 is displayed for $\lambda_{exc} = 632.8$ nm and $I_{exc} = 15.56 \text{ mW cm}^{-2}$. The initial quantum yield of photoconversion is $\phi_{con}(t_{exc} = 0) \approx \phi_{con,Ret_580_{I}}(t_{exc} = 0)\kappa_{Ret_580_{I}} = 0.023$ giving $\phi_{con,Ret_580_{I}}(t_{exc} = 0) \approx 0.056$, as in the top part of Figure 5. After complete photoconversion of Ret_580_I ($t_{exc} > 1$ min), the quantum yield of photoconversion is $\phi_{con}(t_{exc} > 1 \text{ min}, I_{exc} = 15.56 \text{ mW cm}^{-2}) \approx \phi_{con,Ret_580_{II}}(I_{exc} = 15.56 \text{ mW cm}^{-2}) = (4.48 \pm 0.3) \times 10^{-4}$, due to the excitation intensity dependent back photoisomerization of Ret_640 to Ret_580_{II} (see discussion below).

2.3. Fluorescence Behavior

The excitation wavelength dependent fluorescence emission quantum distributions were measured immediately after excitation light switch-off and after sample recovery in the dark. Obtained fluorescence quantum distributions are shown in Figure S14a,b and fluorescence quantum yields are shown in Figure S15 of Section S2 of the Supplementary Materials for the QuasAr1 sample used in the photocycle experiments of Figure 1a ($\lambda_{exc} = 590$ nm, $I_{exc} = 64.65 \text{ mW cm}^{-2}$, and $t_{exc} = 25$ min). Immediately after photoexcitation, the fluorescence quantum efficiency in the fluorescence wavelength region of the photoconversion products turned out to be reduced. After long-time recovery in the dark at room temperature, the fluorescence behavior changed over to the fluorescence behavior of the unexposed samples stored for a long time in the dark at room temperature [33].

The emission wavelength dependent fluorescence excitation quantum distributions of photoexcited QuasAr1 samples were determined after sample recovery in the dark at room temperature. Results are shown in Figure S16 of Section S3 of the Supplementary Materials. The fluorescence excitation spectra behaved similar to the unexposed samples stored for a long time in the dark at room temperature.

3. Discussion

The absorption and emission spectroscopic investigation of the thermal dynamics of the Archaerhodopsin 3 based fluorescent voltage sensor QuasAr1 [33] revealed that fresh thawed samples contained, as covalently bound chromophore, dominantly protonated retinal Schiff base (PRSB) Ret_580 (absorption maximum around 580 nm) with minor amounts of a PRSB isomer absorbing around 450 nm and deprotonated retinal Schiff base (RSB) isomers absorbing below 420 nm. Ret_580 was found to be composed of two isomers, Ret_580_I of mole fraction $\kappa_{Ret_580_{I}} \approx 0.41$ (likely having the 13-*cis* conformation in a specific Apoprotein_I structure) and Ret_580_{II} of mole fraction $\kappa_{Ret_580_{II}} \approx 0.59$ (likely having the all-*trans* conformation in a specific Apoprotein_{II} structure). The photocycle dynamics of Ret_580 were studied experimentally above in Section 2 and in Section S1 of the Supplementary Materials by observing the absorption spectra development during light exposure and after light exposure. The light excitation wavelength and the light excitation intensity were varied.

From the experimental results, we try to resolve the photocycle dynamics of Ret_580_I and Ret_580_{II} and to extract photocycle parameters in the following: The photoexcitation dynamics and the recovery dynamics of Ret_580_I were faster than the photoexcitation dynamics and the recovery dynamics of Ret_580_{II}. These dynamics differences allow the separate characterization of the photocycle dynamics of Ret_580_I and Ret_580_{II}.

Generally, the photoexcitation of rhodopsins causes retinal spatial *cis-trans* isomerization [37,38]. In the rhodopsin photocycle, the photoisomerization of protonated retinal Schiff base (PRSB) is followed by deprotonation to neutral retinal Schiff base (RSB), and the cycle is closed by reprotonation and back isomerization [37–42].

3.1. Photocycle Dynamics of Ret_{580I}

In Figure 6a, a proposed scheme of the photocycle dynamics of the PRSB component Ret_{580I} is shown, and in Figure 7a the corresponding schematic reaction coordinate diagram is depicted. Light absorption excites Ret_{580I} in its S₀ ground state (likely PRSB_{cis}) to a local excited state position LE in the S₁ first excited state (Ret_{580I}*). From there, the S₁ state *cis-trans* isomerization begins along a torsional reaction coordinate via the stationary point SP (Ret_{580I,SP}*), and the funnel state Fu (Ret_{580I,Fu}*) with S₁–S₀ internal conversion (IC) to the S₀ transition state TS₀ (Ret_{580I,TS0}) and further torsion towards the ground-state isomer Ret₅₄₀ (likely PRSB_{trans}). At the TS₀ transition state, there occurs forward *trans* isomerization to Ret₅₄₀ with quantum yield of $\phi_{iso,Ret_{580I}}$ and *cis* back isomerization with quantum yield $\phi_{back,Ret_{580I}} = 1 - \phi_{iso,Ret_{580I}}$. Continued light exposure causes Ret₅₄₀ photoisomerization with excitation to Ret₅₄₀*, S₁ state twisting to Ret_{540,Fu}*, S₁–S₀ internal conversion IC to Ret_{580,TS0}, forward isomerization to Ret_{580I} (quantum yield $\phi_{iso,Ret_{540}}$) and back isomerization to Ret₅₄₀ (quantum yield $\phi_{back,Ret_{540}} = 1 - \phi_{iso,Ret_{540}}$). Ret₅₄₀ (PRSB_{trans}) deprotonates to Ret₄₁₀ (RSB_{trans}) with a relaxation time constant of $\tau_{rel,Ret_{540}}$. Ret₄₁₀ partly recovers back to Ret_{580I} by reprotonation and *trans-cis* isomerization (recovery time $\tau_{rec,Ret_{410} \rightarrow Ret_{580I}}$ and quantum yield of back recovery $\phi_{rec,Ret_{410} \rightarrow Ret_{580I}}$) and it partly relaxes to permanently stable Ret₄₀₀ (RSB_{trans}) caused by thermal apoprotein_I restructuring [33]. The quantum yield of Ret₄₀₀ formation is $\phi_{therm,Ret_{410} \rightarrow Ret_{400}} = 1 - \phi_{rec,Ret_{410} \rightarrow Ret_{580I}}$.

The photodynamics of Ret_{580I} is described in Section S4.1 of the Supplementary Materials. The parameters of the Ret_{580I} photocycle dynamics derived in the analysis are collected in Table 1.

The speed of Ret_{580I} *cis-trans* photoisomerization to Ret₅₄₀ is slowed down by a potential energy barrier along the S₁ state torsional path from the local excited state LE to the funnel state Fu of internal conversion. The time constant of Ret_{580I} *cis-trans* photoisomerization to Ret₅₄₀, $\tau_{iso,Ret_{580I} \rightarrow Ret_{540}}$ is of the order of the Ret₅₈₀ average Strickler–Berg based fluorescence lifetime [43–45] of $\tau_{F,SB,Ret_{580}} \approx 61.5$ ps [33] (separate fluorescence lifetimes for Ret_{580I} and Ret_{580II} were not determined).

The quantum yield of Ret_{580I} → Ret₅₄₀ photoisomerization was found to be rather small and dependent on the photoexcitation wavelength ($\phi_{iso,Ret_{580I}}(590 \text{ nm}) \approx 0.056$, $\phi_{iso,Ret_{580I}}(530 \text{ nm}) \approx 0.023$). The S₁–S₀ internal conversion occurs at a reaction coordinate twist angle of less than 90° favoring the back isomerization to the original state ($\phi_{back,Ret_{580I}}(590 \text{ nm}) = 1 - \phi_{iso,Ret_{580I}}(590 \text{ nm}) \approx 0.944$, $\phi_{back,Ret_{580I}}(530 \text{ nm}) = 1 - \phi_{iso,Ret_{580I}}(530 \text{ nm}) \approx 0.977$).

The metastable Ret₅₄₀ lifetime was found to be $\tau_{rel,Ret_{540}} = 39 \pm 3$ s. Ret₅₄₀ deprotonates to Ret₄₁₀. During light exposure, the population of Ret₅₄₀ accumulates and the light exposure causes photoexcitation and photoisomerization of Ret₅₄₀. The data analysis (Section S4.1 of Supplementary Materials) gives a quantum yield of Ret₅₄₀ forward photoisomerization to Ret_{580I} of $\phi_{iso,Ret_{540}}(590 \text{ nm}) \approx 0.21$ and $\phi_{iso,Ret_{540}}(530 \text{ nm}) \approx 0.125$. The S₁–S₀ internal conversion occurs at a reaction coordinate twist angle of slightly larger than 90° favoring the back isomerization to the original Ret₅₄₀ state ($\phi_{back,Ret_{540}}(590 \text{ nm}) = 1 - \phi_{iso,Ret_{540}}(590 \text{ nm}) \approx 0.79$, $\phi_{back,Ret_{540}}(530 \text{ nm}) = 1 - \phi_{iso,Ret_{540}}(530 \text{ nm}) \approx 0.875$).

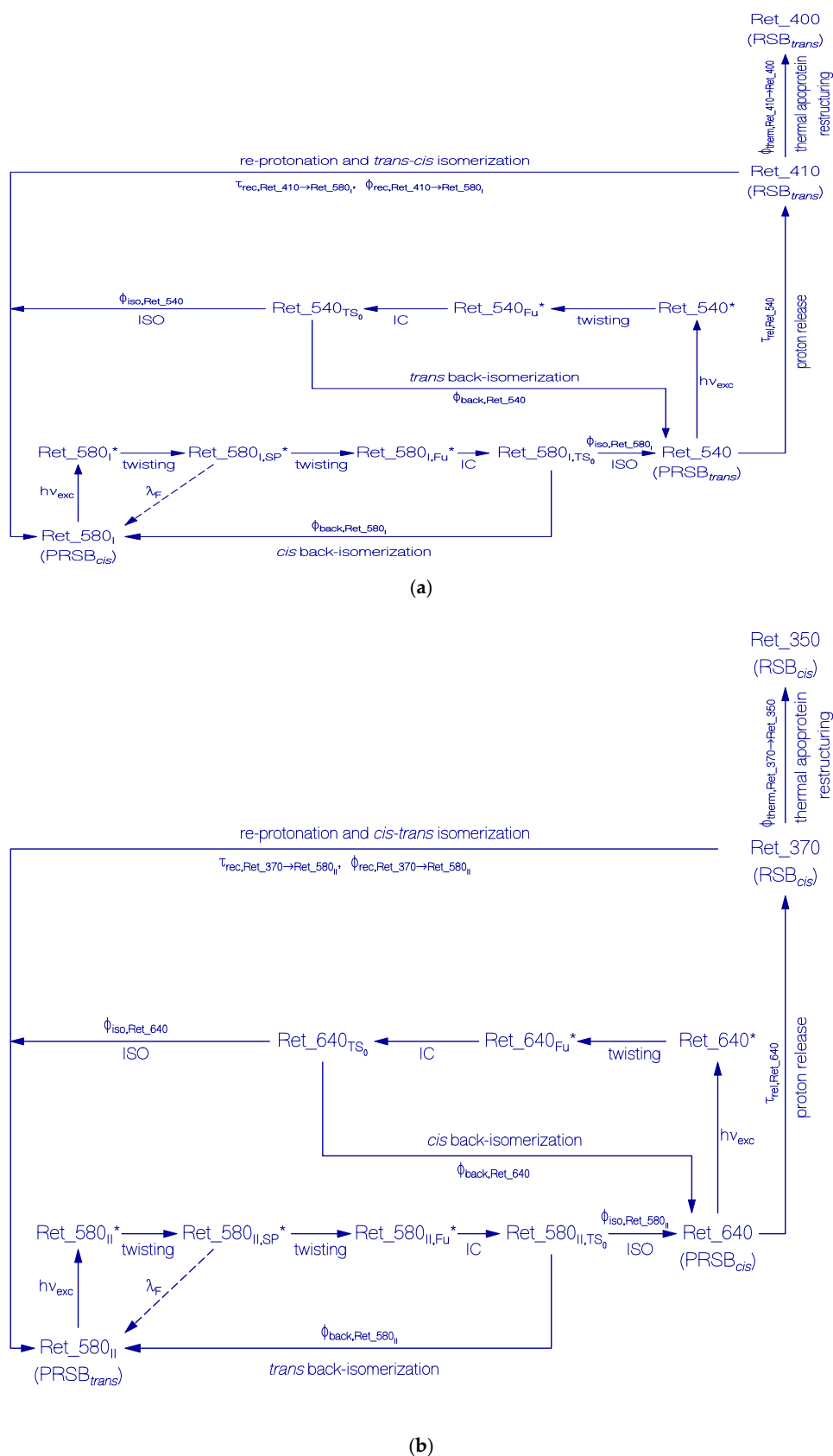
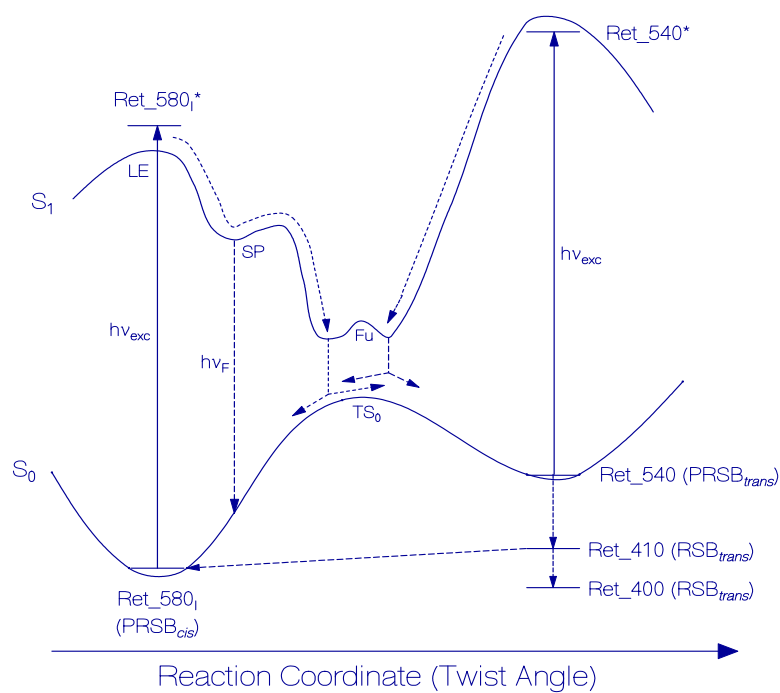
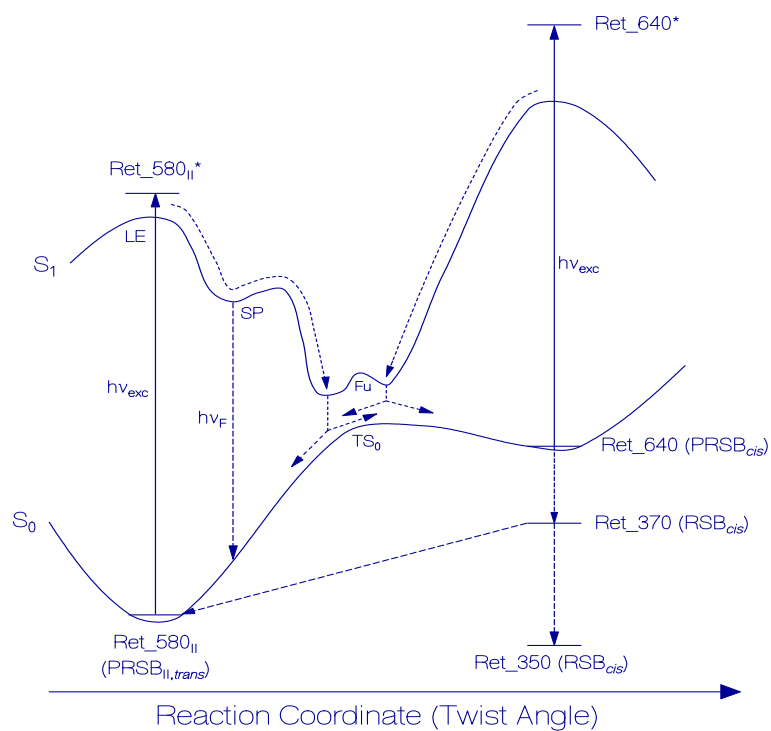


Figure 6. Schemes of photocycle dynamics of retinal components Ret_580_I (a) and Ret_580_{II} (b) of QuasAr1 in pH 8 Tris buffer. IC, internal conversion and ISO, isomerization.



(a)



(b)

Figure 7. Schematic reaction coordinate diagrams for Ret_580_I (a) and Ret_580_{II} (b) photocycles of QuasAr1 in pH 8 Tris buffer.

Table 1. Photodynamics parameters of QuasAr1 in pH 8 Tris buffer.

| Parameter | Value | Comments |
|---|-----------------|---|
| $\kappa_{\text{Ret_580}_I}$ | ≈ 0.41 | [33] |
| $\kappa_{\text{Ret_580}_{II}}$ | ≈ 0.59 | [33] |
| $\lambda_{F,\text{max},\text{Ret_580}}$ (nm) | ≈ 740 | [33] |
| $\tau_{F,\text{SB},\text{Ret_580}}$ (ps) | ≈ 61.5 | [33] |
| $\phi_{\text{iso},\text{Ret_580}_I}$ (590 nm) | 0.056 | Figure 5 and Equation (S23) |
| $\phi_{\text{iso},\text{Ret_580}_I}$ (530 nm) | 0.023 | Figure 5 and Equation (S23) |
| $\phi_{\text{iso},\text{Ret_580}_{II}}$ (590 nm) | 0.00135 | Figure 5 and Equation (S36) |
| $\phi_{\text{iso},\text{Ret_540}}$ (590 nm) | ≈ 0.21 | Figure 5 and Equation (S25) |
| $\phi_{\text{iso},\text{Ret_540}}$ (530 nm) | ≈ 0.125 | Figure 5 and Equation (S25) |
| $\phi_{\text{iso},\text{Ret_640}}$ (590 nm) | ≈ 0.12 | Figure 5 and Equation (S37) |
| $\tau_{\text{rel},\text{Ret_540}}$ (s) | 39 ± 3 | Middle part of Figure 4 and Figure S9 |
| $\tau_{\text{rel},\text{Ret_640}}$ (s) | 17 ± 3 | Bottom part of Figure 4 and Figure S9 |
| $\tau_{\text{rec},\text{Ret_410} \rightarrow \text{Ret_580}_I}$ (632.8 nm) (h) | ≈ 2.6 | Inset of Figure S12 for $\lambda_{\text{pr}} = 580$ nm ($\lambda_{\text{exc}} = 632.8$ nm and $I_{\text{exc}} = 15.65$ mW cm ⁻²) |
| $\tau_{\text{rec},\text{Ret_410} \rightarrow \text{Ret_580}_I}$ (530 nm) (h) | ≈ 0.9 | Inset of Figure S8 for $\lambda_{\text{pr}} = 580$ nm ($\lambda_{\text{exc}} = 530$ nm and $I_{\text{exc}} = 114.2$ mW cm ⁻²) |
| $\tau_{\text{rec},\text{Ret_370} \rightarrow \text{Ret_580}_{II}}$ (632.8 nm) (h) | ≈ 15 | Inset of Figure S12 for $\lambda_{\text{pr}} = 580$ nm ($\lambda_{\text{exc}} = 632.8$ nm and $I_{\text{exc}} = 15.65$ mW cm ⁻²) |
| $\tau_{\text{rec},\text{Ret_370} \rightarrow \text{Ret_580}_{II}}$ (530 nm) (h) | ≈ 8 | Inset of Figure S8 for $\lambda_{\text{pr}} = 580$ nm ($\lambda_{\text{exc}} = 530$ nm and $I_{\text{exc}} = 114.2$ mW cm ⁻²) |
| $\phi_{\text{rec},\text{Ret_410} \rightarrow \text{Ret_580}_I}$ (632.8 nm) | ≈ 0.38 | Figure S12 and Equation (S28) |
| $\phi_{\text{rec},\text{Ret_410} \rightarrow \text{Ret_580}_I}$ (530 nm) | ≈ 0.42 | Figure S8 and Equation (S28) |
| $\phi_{\text{therm},\text{Ret_410} \rightarrow \text{Ret_400}}$ (632.8 nm) | ≈ 0.62 | Figure S12 and Equation (S29) |
| $\phi_{\text{therm},\text{Ret_410} \rightarrow \text{Ret_400}}$ (530 nm) | ≈ 0.58 | Figure S8 and Equation (S29) |
| $\phi_{\text{rec},\text{Ret_370} \rightarrow \text{Ret_580}_{II}}$ (632.8 nm) | ≈ 0.43 | Figure S12 and Equation (S39) |
| $\phi_{\text{rec},\text{Ret_370} \rightarrow \text{Ret_580}_{II}}$ (530 nm) | ≈ 0.64 | Figure S8 and Equation (S39) |
| $\phi_{\text{therm},\text{Ret_370} \rightarrow \text{Ret_350}}$ (632.8 nm) | ≈ 0.57 | Figure S12 and Equation (S40) |
| $\phi_{\text{therm},\text{Ret_370} \rightarrow \text{Ret_350}}$ (530 nm) | ≈ 0.36 | Figure S8 and Equation (S40) |

Abbreviations: $\kappa_{\text{Ret_580}_I}$, fraction of Ret_580_I in Ret_580; $\kappa_{\text{Ret_580}_{II}}$, fraction of Ret_580_{II} in Ret_580; $\lambda_{F,\text{max},\text{Ret_580}}$, wavelength position of maximum fluorescence emission of Ret_580; $\tau_{F,\text{SB},\text{Ret_580}}$, Strickler-Berg based average fluorescence lifetime of Ret_580; $\phi_{\text{iso},\text{Ret_580}_I}$, quantum yield of photoisomerization of Ret_580_I; $\phi_{\text{iso},\text{Ret_580}_{II}}$, quantum yield of photoisomerization of Ret_580_{II}; $\phi_{\text{iso},\text{Ret_540}}$, quantum yield of photoisomerization of Ret_540; $\phi_{\text{iso},\text{Ret_640}}$, quantum yield of photoisomerization of Ret_640; $\tau_{\text{rel},\text{Ret_540}}$, relaxation time constant of Ret_540; $\tau_{\text{rel},\text{Ret_640}}$, relaxation time constant of Ret_640; $\tau_{\text{rec},\text{Ret_410} \rightarrow \text{Ret_580}_I}$, recovery time constant of Ret_410 to Ret_580_I; $\tau_{\text{rec},\text{Ret_370} \rightarrow \text{Ret_580}_{II}}$, recovery time constant of Ret_370 to Ret_580_{II}; $\phi_{\text{rec},\text{Ret_410} \rightarrow \text{Ret_580}_I}$, quantum yield of recovery of Ret_410 to Ret_580_I; $\phi_{\text{rec},\text{Ret_370} \rightarrow \text{Ret_580}_{II}}$, quantum yield of recovery of Ret_370 to Ret_580_{II}; $\phi_{\text{therm},\text{Ret_410} \rightarrow \text{Ret_400}}$, quantum yield of thermal conversion of Ret_410 to Ret_400; and $\phi_{\text{therm},\text{Ret_370} \rightarrow \text{Ret_350}}$, quantum yield of thermal conversion of Ret_370 to Ret_350.

The lifetime $\tau_{\text{rec},\text{Ret_410} \rightarrow \text{Ret_580}_I}$ of the deprotonated retinal Schiff base Ret_410 after excitation light switch-off depended somewhat on the previous excitation light conditions ($\tau_{\text{rec},\text{Ret_410} \rightarrow \text{Ret_580}_I}$ ($\lambda_{\text{exc}} = 632.8$ nm and $I_{\text{exc}} = 15.65$ mW cm⁻²) ≈ 2.6 h, $\tau_{\text{rec},\text{Ret_410} \rightarrow \text{Ret_580}_I}$ ($\lambda_{\text{exc}} = 530$ nm and $I_{\text{exc}} = 114.2$ mW cm⁻²) ≈ 0.9 h). Ret_410 recovers partly back to Ret_580_I by reprotonation and *trans-cis* back isomerization ($\phi_{\text{rec},\text{Ret_410} \rightarrow \text{Ret_580}_I}$ ($\lambda_{\text{exc}} = 632.8$ nm and $I_{\text{exc}} = 15.65$ mW cm⁻²) ≈ 0.38 , $\phi_{\text{rec},\text{Ret_410} \rightarrow \text{Ret_580}_I}$ ($\lambda_{\text{exc}} = 530$ nm and $I_{\text{exc}} = 114.2$ mW cm⁻²) ≈ 0.42). This back recovery process is limited by thermal Apoprotein_I restructuring, thereby lowering the energy level position of the deprotonated retinal Schiff base (RSB_{trans}) below the energy level position of Ret_580_I [33] (changing of metastable Ret_410 to permanently stable Ret_400 with the quantum yields $\phi_{\text{therm},\text{Ret_410} \rightarrow \text{Ret_400}}$ ($\lambda_{\text{exc}} = 632.8$ nm and $I_{\text{exc}} = 15.65$ mW cm⁻²) ≈ 0.62 , $\phi_{\text{therm},\text{Ret_410} \rightarrow \text{Ret_400}}$ ($\lambda_{\text{exc}} = 530$ nm and $I_{\text{exc}} = 114.2$ mW cm⁻²) ≈ 0.58).

3.2. Photocycle Dynamics of Ret_580_{II}

In Figure 6b, a proposed scheme of the photocycle dynamics the PRSB component Ret_580_{II} is shown. In Figure 7b, the corresponding schematic reaction coordinate diagram is depicted. Light absorption excites Ret_580_{II} in its S₀ ground state (likely PRSB_{trans}) to a local excited state position LE in the S₁ first excited state (Ret_580_{II}*). From there, begins the S₁ state *trans-cis* isomerization along a torsional reaction coordinate via the stationary point SP (Ret_580_{II,SP}*), and the funnel state Fu (Ret_580_{II,Fu}*). It follows S₁-S₀ internal conversion IC to the S₀ transition state TS₀ (Ret_580_{II,TS0})

and continued torsion towards the ground-state isomer Ret_640 (likely PRSB_{cis}). At the TS₀ transition state, there occurs forward *cis* isomerization to Ret_640 with a quantum yield of ϕ_{iso,Ret_580II} and *trans* back isomerization with quantum yield of $\phi_{back,Ret_580II} = 1 - \phi_{iso,Ret_580II}$. The continued light exposure causes Ret_640 photoisomerization with excitation to Ret_640*, S₁ state twisting to Ret_640_{Fu}*, S₁-S₀ internal conversion IC to Ret_640_{TS0}, forward isomerization to Ret_580_{II} (quantum yield ϕ_{iso,Ret_640}), and back isomerization to Ret_640 (quantum yield $\phi_{back,Ret_640} = 1 - \phi_{iso,Ret_640}$). Ret_640 (PRSB_{cis}) deprotonates to Ret_370 (RSB_{cis}) with a relaxation time constant of τ_{rel,Ret_640} . Ret_370 partly recovers back to Ret_580_{II} by reprotonation and *cis-trans* isomerization (recovery time $\tau_{rec,Ret_370 \rightarrow Ret_580II}$, quantum yield $\phi_{rec,Ret_370 \rightarrow Ret_580II}$), and it partly relaxes to permanently stable Ret_350 (RSB_{cis}) caused by thermal apoprotein_{II} restructuring [33]. The quantum yield of Ret_350 formation is $\phi_{therm,Ret_370 \rightarrow Ret_350} = 1 - \phi_{rec,Ret_370 \rightarrow Ret_580II}$.

The photodynamics of Ret_580_{II} is described in Section S4.2 of the Supplementary Materials. The parameters of the Ret_580_{II} photocycle dynamics derived in the analysis there are collected in Table 1.

The speed of Ret_580_{II} *trans-cis* photoisomerization to Ret_640 slowed down by a potential energy barrier along the S₁ state torsional path from the local excited state LE to the funnel state Fu of internal conversion. The time constant of Ret_580_{II} *trans-cis* photoisomerization to Ret_640, $\tau_{iso,Ret_580II \rightarrow Ret_640}$ is of the order of the Ret_580 average Strickler–Berg based fluorescence lifetime [43–45] of $\tau_{F,SB,Ret_580} \approx 61.5$ ps [33].

The quantum yield of Ret_580_{II} → Ret_640 photoisomerization was found to be very small ($\phi_{iso,Ret_580II}(590\text{ nm}) \approx 0.00135$). The S₁-S₀ internal conversion occurs at a reaction coordinate twist angle of less than 90° favoring the back isomerization to the original state ($\phi_{back,Ret_580II}(590\text{ nm}) = 1 - \phi_{iso,Ret_580II}(590\text{ nm}) \approx 0.99865$).

The metastable Ret_640 lifetime was found to be $\tau_{rel,Ret_640} = 17 \pm 3$ s. Ret_640 deprotonates to Ret_370. During light exposure, Ret_640 is populated and the light exposure causes photoexcitation and photoisomerization of Ret_640. The data analysis (Section S.4.2 of Supplementary Materials) gives a quantum yield of Ret_640 forward photoisomerization to Ret_580_{II} of $\phi_{iso,Ret_640}(590\text{ nm}) \approx 0.12$. The S₁-S₀ internal conversion occurs at a reaction coordinate twist angle of slightly larger than 90° favoring the back isomerization to the original Ret_640 state ($\phi_{back,Ret_640}(590\text{ nm}) = 1 - \phi_{iso,Ret_640}(590\text{ nm}) \approx 0.88$).

The lifetime $\tau_{rec,Ret_370 \rightarrow Ret_580II}$ of the deprotonated retinal Schiff base Ret_370 after excitation light switch-off depended somewhat on the previous excitation light conditions ($\tau_{rec,Ret_370 \rightarrow Ret_580II}(\lambda_{exc} = 632.8\text{ nm and } I_{exc} = 15.65\text{ mW cm}^{-2}) \approx 15\text{ h}$, $\tau_{rec,Ret_370 \rightarrow Ret_580II}(\lambda_{exc} = 530\text{ nm and } I_{exc} = 114.2\text{ mW cm}^{-2}) \approx 8\text{ h}$). Ret_370 recovers partly back to Ret_580_{II} by reprotonation and *cis-trans* back isomerization ($\phi_{rec,Ret_370 \rightarrow Ret_580II}(\lambda_{exc} = 632.8\text{ nm and } I_{exc} = 15.65\text{ mW cm}^{-2}) \approx 0.43$, $\phi_{rec,Ret_370 \rightarrow Ret_580II}(\lambda_{exc} = 530\text{ nm and } I_{exc} = 114.2\text{ mW cm}^{-2}) \approx 0.64$). This back recovery process is limited by thermal Apoprotein_{II} restructuring, thereby lowering the energy level position of the deprotonated retinal Schiff base (RSB_{cis}) below the energy level position of Ret_580_{II} [33] (changing of metastable Ret_370 to permanently stable Ret_350 with the quantum yields $\phi_{therm,Ret_370 \rightarrow Ret_350}(\lambda_{exc} = 632.8\text{ nm and } I_{exc} = 15.65\text{ mW cm}^{-2}) \approx 0.57$, $\phi_{therm,Ret_370 \rightarrow Ret_350}(\lambda_{exc} = 530\text{ nm and } I_{exc} = 114.2\text{ mW cm}^{-2}) \approx 0.36$).

3.3. Comparison with Other Rhodopsins

The photocycle dynamics of QuasAr1 turned out to be slow and the quantum yield of photoisomerization was found to be low. In Table S1 of the Supplementary Materials (Section S5) quantum yields of primary photoisomerization of some rhodopsins are collected for comparison. The optimization of QuasAr1 for high fluorescence efficiency and high membrane voltage sensitivity lowered the speed of photocycle dynamics and the efficiency of photoisomerization.

4. Experimental

4.1. Sample Preparation

The sample preparation of QuasAr1 was described in [33]. The buffer contained 50 mM Tris-HCl (pH 8), 150 mM NaCl, 0.02% DDM, 0.004% CHS, 0.1 mM PMSE, and 5% glycerol. The expressed QuasAr1 solution was aliquoted to amounts of 30 μ L in Eppendorf tubes, shock-frozen, and stored at -80 °C until they were thawed for experimental investigations. The experiments were carried out at room temperature.

4.2. Spectroscopic Measurements

Transmission measurements, $T(\lambda)$ (λ is the wavelength), were carried out with a spectrophotometer (Cary 50, Varian Australia Pty Ltd., Mulgrave, Victoria, Australia; wavelength resolution 1.5 nm). Attenuation coefficients, $\alpha(\lambda) = -\ln[T(\lambda)]/l$, (l is sample length) were calculated, and absorption coefficients, $\alpha_a(\lambda)$, were determined by subtracting scattering coefficient contributions, $\alpha_s(\lambda)$, according to $\alpha_a(\lambda) = \alpha(\lambda) - \alpha_s(\lambda)$. The scattering coefficient spectrum was approximated by the empirical relation [46] $\alpha_s(\lambda) = \alpha_s(\lambda_0)(\lambda_0/\lambda)^\gamma$ where the wavelength λ_0 is selected in the transparency region and $\gamma \leq 4$ is fitted to the experimental attenuation in the transparency region (for details see [33]).

For the absorption spectroscopic photocycle experiments, QuasAr1 samples were excited with light emitting diodes (LED 590 nm and LED 530 nm from Thorlabs Inc., Newton, NJ, United States) or with a He-Ne laser emitting at 632.8 nm (Model OEM4P, Aerotech Inc., 101 Zeta Drive, Pittsburgh, PA, USA). The sample cell in the spectrophotometer was irradiated transverse to the transmission detection path (exposed area 3×5 mm², sample thickness along excitation path 1.5 mm, and transmission detection path length 3 mm). The excitation power P_{exc} was measured with a power meter (model PD 300-UV-SH photodiode detector head with NOVA power monitor, Ophir Optronics LTD., Science-based Industrial Park, Hartom St 6, Jerusalem, Israel). In the study of the absorption coefficient spectra development, transmission spectra $T(\lambda)$ were recorded repeatedly during the period of light exposure and after light switch-off (data interval 1 nm, averaging time 0.0125 s, recording time for a spectrum from 1100 nm to 200 nm was 11.25 s, the spectra repeating time was set to 18 or 30 s during light exposure and to longer intervals in the observation of the absorption recovery after excitation light switch-off). The temporal development of the absorption behavior of QuasAr1 at selected wavelengths was carried out with a temporal resolution of 12.5 ms.

Fluorescence spectroscopic measurements immediately after the end of photoexcitation and after excitation recovery were carried out with a spectrophotometer (Cary Eclipse, Varian Australia Pty Ltd., Mulgrave, Victoria, Australia). Details of the determination of the fluorescence quantum distributions $E_F(\lambda)$, the fluorescence quantum yields ϕ_F , and the fluorescence excitation quantum distributions $E_{ex}(\lambda)$ are given in [33]. The fluorescence spectroscopic results are presented in Sections S2 and S3 of the Supplementary Materials.

5. Conclusions

The photocycle dynamics of the Archaerhodopsin 3 based fluorescent voltage sensor QuasAr1 from *Halorubrum sodomense* was studied in detail. Its dominant protonated retinal Schiff base Ret_580 absorption band around 580 nm was found to consist of two isomers Ret_580_I (likely a *cis* isomer) and Ret_580_{II} (likely a *trans* isomer) stabilized by different adjacent apoprotein amino acid arrangements. Their slow barrier-involved photoisomerization dynamics in the tens of picosecond regime and the low quantum efficiency of photoisomerization are thought to be responsible for the high fluorescence efficiency and high membrane voltage sensitivity of QuasAr1.

The primary photoisomerization products, Ret_540 (likely PRSB_{trans}) from the educt Ret_580_I, and Ret_640 (likely PRSB_{cis}) from the educt Ret_580_{II}, deprotonate slowly on a time scale of tens of seconds to the neutral retinal Schiff bases Ret_410 and Ret_370, respectively. The long lifetimes of the metastable photoisomers Ret_540 and Ret_640 cause strong excitation intensity dependent back photoisomerization to the primary isomers Ret_580_I and Ret_580_{II}.

The reprotonation and back isomerization of the deprotonated retinal Schiff bases Ret_410 Ret_370 to the original isomers Ret_580_I and Ret_580_{II} occurred on a timescale of several hours. During this long time period, thermal apoprotein restructuring led to a stabilization of the deprotonated retinal Schiff base isomers, Ret_410 to Ret_400 and Ret_370 to Ret_350, leading to an incomplete recovery to the originals Ret_580_I and Ret_580_{II} in the photocycle process.

The performed photocycle studies on QuasAr1 are hoped to be of value for the application of this fluorescent voltage sensor in cell membrane and neuronal function studies.

Supplementary Materials: Supplementary materials can be found at <http://www.mdpi.com/1422-0067/21/1/160/s1>.

Author Contributions: The study was initiated by A.S. and P.H. who expressed, purified and delivered the protein; A.S. carried out initial measurements of the photocycle; A.P. carried out the measurements presented in this paper; The manuscript was written by A.P.; and commented and improved by A.S. and P.H. All authors have read and agreed to the published version of the manuscript.

Funding: This research received no external funding.

Acknowledgments: Alfons Penzkofer thanks Franz J. Gießibl, University of Regensburg, for his kind hospitality. The work was supported by the European Research Council (ERC, MERA project), the DFG Cluster of Excellence “Unifying Systems in Catalysis” EXC314, and the Gottfried Wilhelm Leibniz Prize to Peter Hegemann and Arita Silapetere. Peter Hegemann is supported by the Hertie Foundation.

Conflicts of Interest: The authors declare no conflict of interest.

Abbreviations

| | |
|---------|---|
| Arch | Archaerhodopsin 3 from <i>Halorubrum sodomense</i> |
| FRET | Förster resonance energy transfer |
| GECI | Genetically encoded calcium indicator |
| GEVI | Genetically encoded voltage indicator |
| PRSB | Protonated retinal Schiff base |
| QuasAr | Quality superior to Arch |
| Ret_xxx | Retinal with absorption maximum approximately at xxx nm |
| RSB | Retinal Schiff base |
| Trp | Tryptophan |
| Tyr | Tyrosine |
| VSD | Voltage sensing domain |

Symbols

| Symbol | Unit | Meaning |
|--------------------------|--------------------------|---|
| E_{ex} | | Fluorescence excitation quantum distribution |
| E'_{ex} | cm^{-1} | Normalized fluorescence excitation quantum distribution |
| E_{F} | nm^{-1} | Fluorescence emission quantum distribution |
| I | W cm^{-2} | Intensity |
| I_{exc} | W cm^{-2} | Excitation intensity |
| N | cm^{-3} | Number density |
| $g_{\text{LED xxx nm}}$ | | Spectral light distribution of LED xxx nm |
| n_{ph} | cm^{-3} | Photon number density |
| t | fs, ps, ns, s, min, h, d | Time |
| t_{exc} | S | Exposure time |
| w_{sat} | J cm^{-2} | Saturation energy density |
| Δ | | Difference |
| α | cm^{-1} | Attenuation coefficient |
| α_{a} | cm^{-1} | Absorption coefficient |
| α_{s} | cm^{-1} | Scattering coefficient |
| γ | | Empirical scattering exponent |
| δ | | Difference |
| ϑ | $^{\circ}\text{C}$ | Temperature |
| κ | | Mole fraction |
| λ | Nm | Wavelength |
| λ_{exc} | Nm | Excitation wavelength |
| λ_{F} | Nm | Fluorescence emission wavelength |
| $\lambda_{\text{F,exc}}$ | Nm | Fluorescence excitation wavelength |
| λ_{pr} | Nm | Probe wavelength |
| ν | Hz | Frequency |
| $\tilde{\nu}$ | cm^{-1} | Wavenumber |
| σ | cm^2 | Absorption cross-section |
| τ_{F} | ps, ns | Fluorescence lifetime |
| τ_{rec} | min, h | Recovery time constant |
| τ_{rel} | S | Relaxation time constant |
| τ_{sat} | S | Saturation time constant |
| ϕ | | Quantum yield |
| ϕ_{con} | | Quantum yield of photoconversion |
| ϕ_{F} | | Fluorescence quantum yield |
| ϕ_{iso} | | Quantum yield of photoisomerization |
| ϕ_{therm} | | Quantum yield of thermal conversion |

References

1. Nakajima, R.; Jung, A.; Yoon, B.-J.; Baker, B.J. Optogenetic monitoring of synaptic activity with genetically encoded voltage indicators. *Front. Synaptic Neurosci.* **2016**, *8*, 1–9. [[CrossRef](#)] [[PubMed](#)]
2. Xu, Y.; Zou, P.; Cohen, A.E. Voltage imaging with genetically encoded indicators. *Curr. Opin. Chem. Biol.* **2017**, *39*, 1–10. [[CrossRef](#)] [[PubMed](#)]
3. Knöpfel, T.; Gallero-Salas, Y.; Song, C. Genetically encoded voltage indicators for large scale cortical imaging come of age. *Curr. Opin. Chem. Biol.* **2015**, *27*, 75–83. [[CrossRef](#)] [[PubMed](#)]
4. Nguyen, C.; Upadhyay, H.; Murphy, M.; Borja, G.; Rozsahegyi, E.M.; Barnett, A.; Brookings, T.; McManus, O.B.; Werley, C.A. Simultaneous voltage and calcium imaging and optogenetic stimulation with high sensitivity and a wide field of view. *Biomed. Opt. Express* **2019**, *10*, 789–806. [[CrossRef](#)] [[PubMed](#)]
5. Bando, Y.; Sakamoto, M.; Kim, S.; Ayzenshtat, I.; Yuste, R. Comparative evaluation of genetically encoded voltage indicators. *Cell Rep.* **2019**, *26*, 802–813. [[CrossRef](#)] [[PubMed](#)]

6. Kost, L.A.; Ivanova, V.O.; Balaban, P.M.; Lukyanov, K.A.; Nikitin, E.S.; Bogdanov, A.M. Red fluorescent genetically encoded voltage indicators with millisecond responsiveness. *Sensors* **2019**, *19*, 2982. [[CrossRef](#)] [[PubMed](#)]
7. Bando, Y.; Grimm, C.; Cornejo, V.H.; Yuste, R. Genetic voltage indicators. *BMC Biol.* **2019**, *17*, 71. [[CrossRef](#)]
8. Panzera, L.C.; Hoppa, M.B. Genetically encoded voltage indicators are illuminating subcellular physiology of the axon. *Front. Cell. Neurosci.* **2019**, *13*, 52. [[CrossRef](#)]
9. Kralji, J.M.; Hochbaum, D.R.; Douglass, A.D.; Cohen, A.E. Electrical spiking in *Escherichia coli* probed with a fluorescent voltage-indicating protein. *Science* **2011**, *333*, 345–348. [[CrossRef](#)]
10. Nadeau, J.L. Initial photophysical characterization of the proteorhodopsin optical proton sensor (PROPS). *Front. Neurosci.* **2015**, *9*, 315. [[CrossRef](#)]
11. Tsytsarev, V.; Liao, L.-D.; Kong, K.V.; Liu, Y.-H.; Erzurumlu, R.S.; Olivo, M.; Nitish, N.V. Recent progress in voltage-sensitive dye imaging for neuroscience. *J. Nanosci. Nanotechnol.* **2014**, *14*, 4733–4744. [[CrossRef](#)] [[PubMed](#)]
12. Abdelfattah, A.S.; Kawashima, T.; Singh, A.; Novak, O.; Liu, H.; Shuai, Y.; Huang, Y.-C.; Campagnola, L.; Seeman, S.C.; Yu, J.; et al. Bright and photostable chemigenetic indicators for extended in vivo voltage imaging. *Science* **2019**, *364*, 699–704. [[CrossRef](#)] [[PubMed](#)]
13. Ortiz, G.; Liu, P.; Naing, S.H.H.; Muller, V.R.; Miller, E.W. Synthesis of sulfonated carbofluoresceins for voltage imaging. *J. Am. Chem. Soc.* **2019**, *141*, 6631–6638. [[CrossRef](#)]
14. Mank, M.; Griesbeck, O. Genetically encoded calcium indicators. *Chem. Rev.* **2008**, *108*, 1550–1564. [[CrossRef](#)]
15. Zhong, C.; Schleifenbaum, J. Genetically encoded calcium indicators: A new tool in renal hypertension research. *Front. Med.* **2019**, *6*, 128. [[CrossRef](#)]
16. Siegel, M.S.; Isacoff, E.Y. A genetically encoded optical probe of membrane voltage. *Neuron* **1997**, *19*, 735–741. [[CrossRef](#)]
17. Mutoh, H.; Akemann, W.; Knöpfel, T. Genetically engineered fluorescent voltage reporters. *ACS Chem. Neurosci.* **2012**, *3*, 585–592. [[CrossRef](#)]
18. St-Pierre, F.; Chavarha, M.; Lin, M.Z. Design and sensing mechanisms of genetically encoded fluorescent voltage indicators. *Curr. Opin. Chem. Biol.* **2015**, *27*, 31–38. [[CrossRef](#)]
19. Yi, B.; Kang, B.E.; Lee, S.; Braubach, S.; Baker, B.J. A dimeric fluorescent protein yields a bright, red-shifted GEVI capable of population signals in brain slice. *Sci. Rep.* **2018**, *8*, 15199. [[CrossRef](#)]
20. Jin, L.; Han, Z.; Plasisa, J.; Wooltorton, J.R.A.; Cohen, L.B.; Pieribone, V.A. Single action potentials and subthreshold electrical events imaged in neurons with a novel fluorescent protein voltage probe. *Neuron* **2012**, *75*, 779–785. [[CrossRef](#)]
21. Gong, Y. The evolving capabilities of rhodopsin-based genetically encoded voltage indicators. *Curr. Opin. Chem. Biol.* **2015**, *27*, 84–89. [[CrossRef](#)] [[PubMed](#)]
22. Venkatachalam, V.; Brinks, D.; Maclaurin, D.; Hochbaum, D.R.; Kralj, J.M.; Cohen, A.E. Flash memory: Photochemical imprinting of neuronal action potentials onto a microbial rhodopsin. *J. Am. Chem. Soc.* **2014**, *136*, 2529–2537. [[CrossRef](#)] [[PubMed](#)]
23. Hashemi, N.A.; Bergs, A.C.F.; Schüler, C.; Scheiwe, A.R.; Costa, W.S.; Bach, M.; Liewald, J.F.; Gottschalk, A. Rhodopsin-based voltage imaging tools for use in muscles and neurons of *Caenorhabditis elegans*. *Proc. Natl. Acad. Sci. USA* **2019**, *116*, 17051–17060. [[CrossRef](#)]
24. Gong, Y.; Huang, C.; Li, J.Z.; Grewe, B.F.; Zhang, Y.; Eismann, S.; Schintzer, M.J. High-speed recording of neural spikes in awake mice and flies with a fluorescent voltage sensor. *Science* **2015**, *350*, 1361–1366. [[CrossRef](#)]
25. Kannan, M.; Vasan, G.; Huang, C.; Haziza, S.; Li, J.Z.; Inan, H.; Schnitzer, M.J.; Pieribone, V.A. Fast, in vivo voltage imaging using red fluorescent indicator. *Nat. Method* **2018**, *15*, 1108–1116. [[CrossRef](#)]
26. Hochbaum, D.R.; Zhao, Y.; Farhi, S.L.; Klapoetke, N.; Werley, C.A.; Kapoor, V.; Zou, P.; Kralj, J.M.; Maclaurin, D.; Smedemark-Margulies, N.; et al. All-optical electrophysiology in mammalian neurons using engineered microbial rhodopsins. *Nat. Methods* **2014**, *11*, 825–833. [[CrossRef](#)]
27. Lou, S.; Adam, Y.; Weinstein, E.N.; Williams, E.; Williams, K.; Parot, V.; Kavokine, N.; Liberles, S.; Madisen, L.; Zeng, H.; et al. Genetically targeted all-optical electrophysiology with a transgenic Cre-dependent Optopatch mouse. *J. Neurosci.* **2016**, *36*, 11059–11073. [[CrossRef](#)]

28. Adam, Y.; Kim, J.J.; Lou, S.; Zhao, Y.; Xie, M.E.; Brinks, D.; Wu, H.; Mostajo-Radji, M.A.; Kheifets, S.; Parot, V.; et al. Voltage imaging and optogenetics reveal behaviour-dependent changes in hippocampal dynamics. *Nature* **2019**, *569*, 413–417. [[CrossRef](#)]
29. Kralj, J.M.; Douglass, A.D.; Hochbaum, D.R.; Maclaurin, D.; Cohen, A.E. Optical recording of action potentials in mammalian neurons using microbial rhodopsin. *Nat. Methods* **2012**, *9*, 90–95. [[CrossRef](#)]
30. Gong, Y.; Li, J.Z.; Schnitzer, M.J. Enhanced Archaelhodopsin fluorescent protein voltage indicators. *PLoS ONE* **2013**, *8*, e66959. [[CrossRef](#)]
31. Flytzanis, N.C.; Bedbrook, C.N.; Engqvist, M.K.M.; Xiao, C.; Chan, K.Y.; Sternberg, P.W.; Arnold, F.H.; Gradinaru, V. Archaelhodopsin variants with enhanced voltage-sensitive fluorescence in mammalian and *Caenorhabditis elegans* neurons. *Nat. Commun.* **2014**, *5*, 4894. [[CrossRef](#)]
32. Piatkevich, K.D.; Jung, E.E.; Straub, C.; Linghu, C.; Park, D.; Suk, H.J.; Hochbaum, D.R.; Goodwin, D.; Pnevmatikakis, E.; Pak, N.; et al. A robotic multidimensional directed evolution approach applied to fluorescent voltage reporters. *Nat. Chem. Biol.* **2018**, *14*, 352–360. [[CrossRef](#)] [[PubMed](#)]
33. Penzkofer, A.; Silapetere, A.; Hegemann, P. Absorption and emission spectroscopic investigation of the thermal dynamics of the Archaelhodopsin 3 based fluorescent voltage sensor QuasAr1. *Int. J. Mol. Sci.* **2019**, *20*, 4086. [[CrossRef](#)] [[PubMed](#)]
34. Eichler, H.J.; Günter, P.; Pohl, D.W. *Laser-Induced Dynamic Gratings*; Springer: Berlin/Heidelberg, Germany, 1986; pp. 38–93.
35. Käding, O.W.; Skurk, H.; Maznev, A.A.; Matthias, E. Transient thermal gratings at surfaces for thermal characterization of bulk materials and thin films. *Appl. Phys. A* **1995**, *61*, 253–261. [[CrossRef](#)]
36. Zirak, P.; Penzkofer, A.; Lehmpfuhl, C.; Mathes, T.; Hegemann, P. Absorption and emission spectroscopic characterization of blue-light receptor Slr1694 from *Synechocystis* sp. PCC6803. *J. Photochem. Photobiol. B Biol.* **2007**, *86*, 22–34. [[CrossRef](#)]
37. Ernst, O.P.; Lodowski, D.T.; Elstner, M.; Hegemann, P.; Brown, L.S.; Kandori, H. Microbial and animal rhodopsins: Structures, functions, and molecular mechanisms. *Chem. Rev.* **2014**, *114*, 126–163. [[CrossRef](#)]
38. Penzkofer, A.; Hegemann, P.; Kateriya, S. Organic dyes in optogenetics. In *Organic Lasers and Organic Photonics*; Duarte, F.J., Ed.; IOP Publishing: Bristol, UK, 2018; pp. 13–1–13–114.
39. Longstaff, C.; Calhoun, R.D.; Rando, R.R. Deprotonation of the Schiff base of rhodopsin is obligate in the activation of the G protein. *Proc. Natl. Acad. Sci. USA* **1986**, *83*, 4209–4213. [[CrossRef](#)]
40. Lanyi, J.K.; Schobert, B. Crystallographic structure of the retinal and the protein after deprotonation of the Schiff base: The switch in the bacteriorhodopsin photocycle. *J. Mol. Biol.* **2002**, *321*, 727–737. [[CrossRef](#)]
41. Kubli-Garfias, C.; Salazar-Salinas, K.; Perez-Angel, E.C.; Seminario, J.M. Light activation of the isomerization and deprotonation of the protonated Schiff base retinal. *J. Mol. Model.* **2011**, *17*, 2539–2547. [[CrossRef](#)]
42. Lanyi, J.K. Bacteriorhodopsin. *Annu. Rev. Physiol.* **2004**, *66*, 665–688. [[CrossRef](#)]
43. Strickler, S.J.; Berg, R.A. Relationship between absorption intensity and fluorescence lifetime of molecules. *J. Chem. Phys.* **1962**, *37*, 814–822. [[CrossRef](#)]
44. Birks, J.B.; Dyson, D.J. The relations between the fluorescence and absorption properties of organic molecules. *Proc. R. Soc. Lond. Ser. A* **1963**, *275*, 135–148.
45. Deshpande, A.V.; Beidoun, A.; Penzkofer, A.; Wagenblast, G. Absorption and emission spectroscopic investigation of cyanovinyl-diethylaniline dye vapors. *Chem. Phys.* **1990**, *142*, 123–131. [[CrossRef](#)]
46. Penzkofer, A.; Shirdel, J.; Zirak, P.; Breitzkreuz, H.; Wolf, E. Protein aggregation studied by forward light scattering and transmission analysis. *Chem. Phys.* **2007**, *342*, 55–63. [[CrossRef](#)]

